Summer 2016

Attenuation properties of cement composites: Experimental measurements and Monte Carlo calculations

Raul Florez

Department:

ATTENUATION PROPERTIES OF CEMENT COMPOSITES:

EXPERIMENTAL MEASUREMENTS AND MONTE CARLO CALCULATIONS

by

RAUL FERNANDO FLOREZ MEZA

A THESIS

Presented to the Faculty of the Graduate School of the

MISSOURI UNIVERSITY OF SCIENCE AND TECHNOLOGY

In Partial Fulfillment of the Requirements for the Degree

MASTER OF SCIENCE IN NUCLEAR ENGINEERING

2016

Approved by

Ayodeji Alajo, Advisor
Carlos Castano
Henry Colorado

PUBLICATION THESIS OPTION

This thesis consists of the following two articles, formatted in the style used by the Missouri University of Science and Technology:

Pages 16-37 are intended for submission to the JOURNAL OF NUCLEAR MATERIALS.

Pages 38-51 are intended for submission in JOURNAL OF CONSTRUCTION AND BUILDING MATERIALS.

ABSTRACT

Developing new cement based materials with excellent mechanical and attenuation properties is critically important for both medical and nuclear power industries. Concrete continues to be the primary choice material for the shielding of gamma and neutron radiation in facilities such as nuclear reactors, nuclear waste repositories, spent nuclear fuel pools, heavy particle radiotherapy rooms, particles accelerators, among others. The purpose of this research was to manufacture cement pastes modified with magnetite and samarium oxide and evaluate the feasibility of utilizing them for shielding of gamma and neutron radiation. Two different experiments were conducted to accomplish these goals. In the first one, Portland cement pastes modified with different loading of fine magnetite were fabricated and investigated for application in gamma radiation shielding. The experimental results were verified theoretically through XCOM and the Monte Carlo N-Particle (MCNP) transport code. Scanning electron microscopy and x-ray diffraction tests were used to investigate the microstructure of the samples. Mechanical characterization was also perfornmed by compression testing. The results suggest that fine magnetite is a suitable aggregate for increasing the compressive and flexural strength of white Portland cement pastes; however, there is no improvement of the attenuation at intermediate energy (662 keV). For the second experiment, cement pastes with different concentrations of samarium oxide were fabricated and tested for shielding against thermal neutrons. MCNP simulations were used to validate the experimental work. The result shows that samarium oxide increases the effective thermal cross section of Portland cement and has the potential to replace boron bearing compounds currently used in neutron shielding.

ACKNOWLEDGMENTS

I would like to express my sincere gratitude to my committee members Dr. Ayodeji Alajo, Dr. Carlos Castano and Dr. Henry Colorado for the continuous support of my master study and related research. Certainly, this work would not been possible without their guidance, patience, motivation and immense knowledge. I would also like to thank the professors of the Nuclear Engineering program at Missouri S&T, especially Dr. Joseph Graham who always took the time to discuss questions about my research and whose insights were really helpful to my work.

I am also grateful to the staff at the Missouri S&T nuclear reactor that helped me to conduct the neutron attenuation measurements. Bill, Craig and Anthony were always willing to put in extra hours to help me to complete my project. Thanks to my fellow graduate students and friends at Missouri S&T for making the last two years one of the most memorable and enriching time of my life.

Finally, I thank my family for their unconditional support in every endeavor I have undertaken through my life. In particular I would like to thank my parents, Raul Florez and Ingrid Meza, to whom I dedicate this thesis.

TABLE OF CONTENTS

Page

LIST OF ILLUSTRATIONS

Page

SECTION

PAPER I

PAPER II

LIST OF TABLES

Page

SECTION

PAPER I

PAPER II

1. INTRODUCTION

1.1. SCOPE OF THE WORK

Concrete is the most common shielding material for ionizing radiation. It is extensively used in facilities such as nuclear reactors, spent nuclear fuel repositories, particle accelerators, radiotherapy rooms, among others. As a shielding material, concrete is very attractive because its attenuation properties which can be easily tailored by controlling its chemical composition. Moreover, concrete has relative inexpensive fabrication cost and can be cast in many complex forms exhibiting good mechanical, structural and physicochemical properties. All these characteristics make concrete a suitable material for the aforementioned shielding applications.

There has been extensive work about the optimization of the key properties of concrete for shielding applications in both nuclear and medical industries. An important area of research has look at the improvement of radiation shielding properties through the use of admixtures. They are ingredients added in small proportion to modify primarily the structural strength and the radiation capacity of concrete. While much effort has been spent studying the effect of coarse aggregates, relatively little is known about the effect of using nano and fine aggregates on the final properties of radiation shielding concrete (RSC). Therefore, any attempt to contribute to the understanding of radiation shielding in concrete modified with these types of aggregates is helpful for the radiation shielding community.

Studying the effect of nano and fine aggregates on the properties of concrete is a very broad research topic. In order to make the objectives of this work more focused and achievable, this research is particularly concerned with the effect of adding fine magnetite and samarium oxide powders on the structural, mechanical and attenuation properties of white ordinary Portland cement pastes. The study was done using a combination of experimental and simulation techniques. The experimental techniques were used to characterize the structural properties of the composites, measure the stress-strain curves of the samples and determine their attenuation properties. The simulations were performed to make comparisons with the radiation transmission experiments and predict the attenuation properties of the studied composites.

1.2. RESEARCH OBJECTIVES

The following were the objectives for this work:

- Fabricate cement samples with different content of magnetite and samarium oxide powders.
- Perform structural and mechanical characterization of the fabricated composites.
- Investigate the attenuation properties of the cement samples exposed to neutrons and gamma rays.
- To perform numerical simulations in MCNP to predict the attenuation properties of the cement composites.

1.3. MAIN CONTRIBUTIONS

Even though more experimental work will have to be conducted in the future to improve our understanding of the attenuation properties of cement composites, the objectives of the present work were accomplished and the information revealed contributes to the knowledge of nuclear radiation shielding. In summary, this work present evidence that the addition of fine magnetite powder could improve the mechanical properties of cement based materials, particularly their compression and tensile strengths. However, the use of fine magnetite is not a suitable option for shielding gamma radiation since it decreases the density of the composites and does not enhance the attenuation properties significantly at the photon energies commonly encountered in nuclear applications. On the other hand, mineral admixtures of samarium oxide proved to be effective for enhancing the attenuation properties of cement composites against thermal neutrons.

1.4. ORGANIZATION OF THESIS

The next sections of this thesis are summarized as follows:

- Section 2: Background contains a comprehensive survey of the scientific literature of relevance to this study. This section includes basic information on ionizing radiation, interactions of neutrons and gamma rays with matter, Monte Carlo simulations, and the use of concrete as a shielding material. The main purpose of this section is to introduce some basic concepts and terminology found in the

other sections and to frame the activities performed in this work within the current understanding of radiation shielding concrete.

- Section 3: Papers contains the two manuscripts about the experiments that were conducted in this research. The first paper gives information about the mechanical, structural and gamma ray attenuation properties of cement composites modified with magnetite. The second one describes the attenuation properties of samarium oxide-cement composites against thermal neutron. Both papers described in detailed the experimental techniques that were used in this study as well as the main findings.
- Section 4: Conclusions and Future work presents a summary of the work and discusses its main findings and limitations. This section also outlines directions for future experimental and simulation work.

2. BACKGROUND

2.1. IONIZING RADIATION AND SHIELDING

Ionizing radiation is an umbrella term for particles (neutrons, alpha/beta, protons and electrons) and electromagnetic waves (X-rays and gamma rays) which carry enough energy to remove bound electrons from atoms and molecules [1]. This kind of radiation plays an important role in several industries, including but not limited: military, medical, aerospace and nuclear power industries. Table 2.1 shows some sources and characteristics of the types of ionizing radiation commonly encountered in some the aforementioned industries. Despite its widespread use, prolonged or accumulated exposure to ionizing radiation can be detrimental to human beings and therefore especial measures must be taken to prevent unwanted exposure to it. The most effective method to minimize exposure to external radiation hazards involves the correct use of time, distance and shielding [1]. Minimizing the time spend in the proximity to radioactive sources, maximizing the distance between the source and exposed person, and using suitable shielding is the best way to guarantee radiation protection. Among these strategies, shielding is of particular importance because it is the only viable option in many situations.

The practice of radiation shielding consists in placing a barrier between the external radioactive source and the receptor. By doing this, some or all the amount of the radiation emitted by the source will be scattered or absorbed by the constitutive atoms of the shielding material. This process is called attenuation and is the fundamental physical principle upon which radiation shielding is based. The attenuation capability of a given material is strongly dependent on the type of radiation and the range of energies associated with the radiation. Therefore, design and construction of effective radiation shields require an in-depth knowledge of the types of interaction between radiation and the target material.

2.2. INTERACTION OF RADIATION WITH MATTER

In general, ionizing radiation can be categorized into two big groups. The first one includes all charged particles such as heavy ions, electrons, protons and alpha particles,

which interact with matter primarily through Coulombic forces [2]. This kind of radiation is called directly ionizing radiation and it is relatively easy to shield because of the low penetrating power associated to charged particles. On the other hand, there is a second type of ionizing radiation consisting of high energy photons and neutrons which are electrically neutral. They interact with matter by different electromagnetic mechanisms producing indirect ionization of atoms[2]. Indirectly ionizing radiations pass easily through most materials and hence they are relatively difficult to shield as compared to charged particles. The mechanisms by which neutrons and photons interact with matter are summarized next section.

Table 2.1 Types of ionizing radiation encountered in different industries [3]

Industry	**Radiation Sources**	**Composition**	**Typical Energy Range**
Aerospace	i. Galactic Cosmic Rays (GCR). ii. Solar particle events (SPE). iii. Trapped particle belts.	GCR consist of high-energy protons (85%), alpha particles (14%) and heavy nuclei (1%). SPE consist of transient burst of low to medium energy protons and alpha particles. Trapped radiation belts mainly consist of high energy electrons and protons.	i. 10 MeV to 10 GeV. ii. Few MeV to 100s MeV. iii. Electrons: few MeV and protons: several 100s of MeV.
Medical Radiology, Interventional and Radiotherapy	i. X-rays and γ-rays. ii. Protons and electrons.	Electromagnetic radiation: wide range of X-rays and γ-rays. Particle radiation: for therapeutic purposes.	Tens of keV to tens of MeV.
Nuclear Reactors	i. Particle emissions ii. γ-rays.	Neutrons, alpha and beta particles, and γ-rays.	i. 0 to 15 MeV for neutrons, 0 to 4 MeV for alpha and beta particles. ii. 10 keV to 3 Mev.

2.2.1. Photon Interactions and Cross Sections. In theory, there are 12 different processes by which the electromagnetic field of a gamma ray may interact with matter

[4]. Only three of these mechanisms play an important role at relatively low energies (<10 MeV) commonly encountered in nuclear shielding applications, they are:

- *Photoelectric effect:* The photoelectric process involves the complete transfer of the incident photon energy to an atomic electron and its ejection from the atom. Photoelectrons can only occur when the photon energy (hv) is larger than the binding energy (E_b) of atomic electrons. The photoelectric process can be represented by the following reaction:

$$\gamma + X \rightarrow X^+ + e \tag{1}$$

where X is the target atom, which gets an overall positive charge when the electron e is knocked off from one of its shells by the incident gamma ray photon γ. It is difficult to use quantum mechanics principles to calculate the exact cross section of photoelectric interactions because of the complexity of the Dirac wave functions for atomic electrons. Despite this limitation, theoretical estimates and experimental studies have found that there is a strong dependence of the total photoelectric cross section upon the atomic number of the target material (Z) and the energy of the incident photon (E_γ) . A crude but useful approximation for the photoelectric cross section is given as follows:

$$\tau \propto \frac{Z^n}{E_\gamma^{3.5}} \tag{2}$$

This equation suggests that the probability of photoelectric effect increases rapidly with atomic number of the target atom and decreases sharply with higher incident photo energy. Consequently, this process is especially effective for attenuation of low energy gamma photons using heavy atoms.

- *Compton effect:* This attenuation mechanism refers to the inelastic scattering of photons from free or loosely bound electrons which are at rest [5]. The energy of the incident photon is shared between the scattered photon and the kinetic energy of the recoil electron. The probability for a Compton scattering interaction was obtained by Klein and Nishima in 1929 using electrodynamics quantum theory. They derived an adequate quantum-mechanical description for Compton scattering and found an expression for the differential collision cross section which is now known as the Klein-Nishima equation. The Compton scattering probability (σ), is almost independent of the

atomic number Z, decreases as the photon energy increases and is directly proportional to the number of electrons per gram.

- *Pair production:* Above incident photon energies of 1.02 MeV, pair production becomes increasingly important. In this interaction the photon is completely absorbed and in its place appears a positron-negatron pair. The process occurs only in the field of charged particles, mainly the nuclear field but also to some degree in the field of an electron. The presence of this particle is necessary to ensure momentum conservation. Pair production in the vicinity of a nucleus can be represented as follows:

$$\gamma + X \rightarrow e + e^{+} + X^{*} \tag{3}$$

where X and X^{*} represent the ground and excited state of a heavy nucleus. The probability of occurrence of this process is given by the Pair production cross section which can be calculated from quantum electrodynamics using Dirac's relativistic theory of the electron. Theoretical values of pair production cross sections in the Coulombic field of the nucleus have been calculated by Bethe and Heitler [6] using plane wave (PW) approximation. However, this approximation is not valid for high Z elements or for low Z elements in the low energy region and therefore "Coulombs corrections" need to be bone to the PW calculation. Pair production probability (κ) increases with increasing photon energy and has a roughly Z^2 dependance.

For a given material, each of the above-mentioned effects plays a predominant role within a specific range of γ ray energies. The relative importance of σ, τ and κ is shown graphically in Figure 2.1. Photoelectric collisions are important only for small hv and large Z, pair production is of major importance only for large hv and large Z, and Compton collisions predominate in the entire domain of intermediate hv, for all Z.

2.2.1.1. Linear attenuation coefficient. The decrease in intensity of a photon beam crossing an absorber material is determined by the Lambert-Beer law which can be expressed as follows:

$$I = I_0 e^{-\mu_t x} \tag{4}$$

where I_0 is the intensity of the photon beam just before it enters the material and I is the intensity at a depth x. The parameter μ_t is known as the total linear attenuation coefficient and determines how quickly or slowly a certain photon beam will attenuate

while passing through a material. The linear attenuation coefficient is a function not only of the photon energy but also of the type and density of the material.

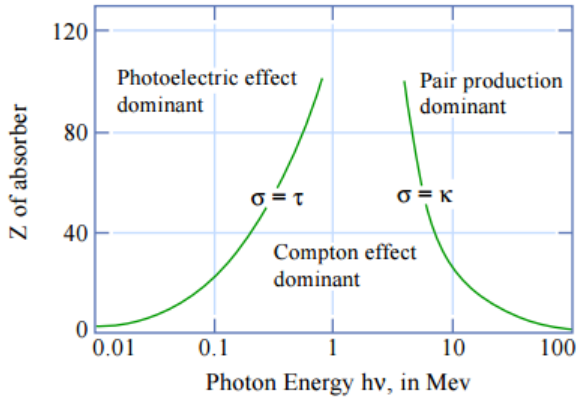

Figure 2.1 Relative importance of the three majors types of γ-ray interaction [7]

It is possible to measure experimentally the linear attenuation coefficient of a given absorber. To do so, it is just necessary to measure the incoming and outgoing intensities of a photon beam that passes through a slab of thickness x. Figure 2.2 illustrates the common experimental arrangement for measuring the total attenuation coefficient. A narrow beam of photons is defined by circular apertures in two or more massive shields, or collimators. When the chosen absorber is placed in the beam, and between the collimators, all photons that are coherently or incoherently scattered by a few degrees are prevented from reaching the detector, as are nearly all secondary photons from photo and pair encounters in the absorber.

2.2.1.2. Mass attenuation coefficient. For any type of interaction, the mass attenuation coefficient is the linear attenuation divided by the density. The mass attenuation coefficients are really of more fundamental value than are the linear attenuation coefficients, because all mass attenuation coefficients are independent of the actual density and physical state of the absorber.

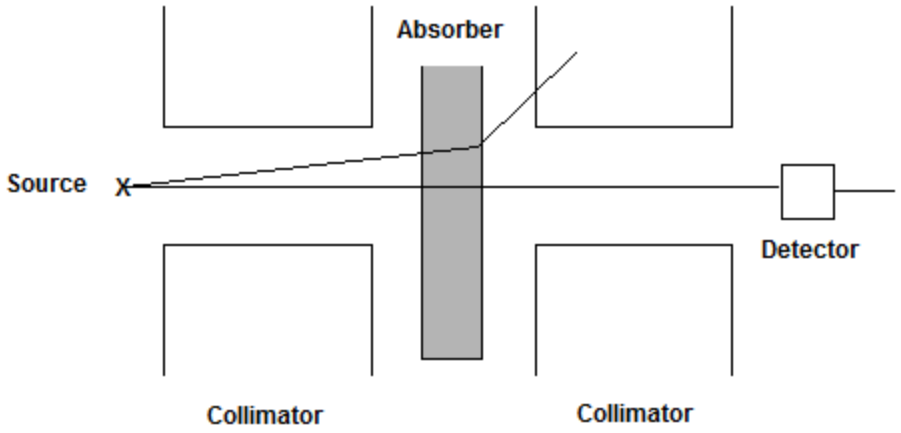

Figure 2.2 Typical arrangements of source, absorber and detector in ideal "narrow beam" for determination of linear attenuation coefficient

2.2.2. Interaction of Neutrons with Matter. Neutrons do not interact with the electric field of the atoms because they do not have an effective electric charge. Nonetheless, neutrons do feel the strong nuclear force of the nuclei and they can interact with it through different mechanisms. Among all the possible interaction processes for neutrons, only the following four are important for radiation shielding applications:

- *Elastic scattering:* This process is the principal type of interaction of neutrons with atomic nuclei and the most important one for slowing down neutrons (Moderation). A neutron scattering reaction occurs when the target nucleus emits a single neutron after neutron-nucleus interaction. In an elastic scattering reaction between a neutron and a target nucleus, there is no energy transferred into nuclear excitation. The elastic scattering conserves both momentum and kinetic energy of the system. There is usually some transfer of kinetic energy from the incident neutron to the target nucleus. The target nucleus gains the same amount of kinetic energy that the neutron loses. For a neutron of kinetic energy E encountering a nucleus of atomic weight A, the average energy loss is given by:

$$\frac{2EA}{(A+1)^2} \tag{5}$$

This equation shows that in order to reduce the speed of neutrons with the fewest number of elastic collisions, target nuclei with small A should be used. For this reason light weight elements like hydrogen are used in neutron radiation shields to thermalize fast neutrons that can be subsequently absorbed by the other elements of the shield.

- *Inelastic scattering:* In an inelastic scattering reaction between a neutron and a target nucleus some of the energy of the incident neutron is absorbed to the recoiling nucleus and the nucleus remain in an excited state. The nucleus gives up excitation energy by emitting one or more gamma rays to reach its ground state. Inelastic scattering occurs above a threshold energy. This threshold is given by the following equation:

$$E_t = (\frac{A+1}{A}) \times \varepsilon_1 \quad (6)$$

where E_t is the inelastic threshold energy ε_1 is the first excited energy state of the nucleus and A is the mass number of the nuclei. In general, the energy of the first excited state of nuclei decreases with increasing mass number. Therefore, an inelastic scattering plays an important role in slowing down neutrons especially at high energies and by heavy nuclei.

- *Transmutation:* In this kind of reaction an element changes into another one when a neutron is absorbed by a nucleus. Transmutation reactions can be induced by neutrons of all energies and they are important in neutron shielding applications to understand the depletion of neutron absorber used commonly in radiation of thermal neutrons. For example, one transmutation reaction of interest for neutron shielding is the depletion of Boron-10 which is used as an aggregate in shielding applications due to its high neutron cross section. When a B-10 nucleus captures a slow neutron it transforms into Lithium-7 and emits an $\propto$-particle:

$$n + B_5^{10} \rightarrow Li_3^7 + \alpha \quad (7)$$

This transmutation reaction changes not only the attenuation capability of the shielding material but also introduces structural changes that can affect the long term stability of the shielding [8].

- *Radioactive Capture*: It is a very common type of reaction in which a nucleus absorbs the neutron and goes into an excited state. To return to the stable state, the nucleus emits gamma rays. In this case no transmutation occurs, however the isotopic

form of the element changes due to increase in the number of neutron. This reaction can be represented by the following equation:

$$n + X_p^{n+p} \rightarrow X_p^{n+p+1} + \gamma \quad (8)$$

Radioactive capture reactions are important in shielding applications because they usually determine the final radioactivity of the shielding material after it has been exposed to neutron irradiation. Materials used for shielding of neutrons accumulate radioisotopes induced by neutron capture reactions and this radioactivity is a primary concern at both operational and dismantling stage of the shielding facility [9-10]. Therefore, it is important to consider these kinds of reactions when designing neutron shields to retain little residual activity.

2.3. CONCRETE AS RADIATION SHIELDING MATERIAL

Concrete is a hard compact material formed when a mixture of cement, sand, gravel and water undergoes hydration [11]. This composite is considered to be an excellent and versatile shielding material with various applications in nuclear power plants, particle accelerators, research reactors, nuclear repositories, nuclear waste containers, laboratory hot cells and medical facilities. The main advantage of using concrete as a shielding material is the ability to tailor the attenuation characteristics by varying its chemical composition. Additionally, concrete is a relative inexpensive material and can be easily handled and cast into complex shapes.

The shielding capabilities of concretes are usually controlled by the addition of mineral admixtures in the form of fine and coarse aggregates. ASTM C638 standard provides two classes of aggregates for use in radiation shielding concrete. The first class includes all minerals and rocks with high specific gravity that are suitable for gamma ray attenuation. The second group consists of minerals and rocks which are particularly effective in absorbing neutrons without highly penetrating gamma rays. Table 2.2 summarizes the most commonly natural occurring aggregates used for gamma ray and neutron shielding. Besides natural occurring minerals, manufactured aggregates such as iron, steel balls, steel punch and other additives can be also used to enhance the capability of concrete to attenuate neutrons and gamma rays.

Many authors have investigated the attenuation properties of concrete with addition of both natural and artificial aggregates. As for shielding of gamma radiation, the studies suggest the feasibility of using a wide variety of coarse aggregates including: ilmenite [12], hematite [13], barite [14], limonite[15], lime[16], magnetite [17], galena[18], lead [19] and steel slags [20]. There are also many studies which focused on increasing the attenuation coefficient of concrete for neutrons with different additives such as boric compounds[21-22], rare earths [23-26] and polymers [27].

Table 2.2 Commonly used aggregates for RSC (Modified from ASTM C638)

Class	Aggregates
Gamma Ray Shielding (Class 1)	• *Iron Minerals*: Hematite, Ilmenite, Geothite, Limonite, Magnetite, Lepidocrocite. • *Barium Minerals:* WItherite, Barite • Ferrophosporous
Neutron Shielding (Class 2)	• Boron containing materials: Borax, Kernite, Colemanite, Sassolite, Tricalconite, Priceite, Inyoite, Hydroboracite, Szaibelyite

Recent investigations have also shown that the size of the aggregates affects the final properties of the radiation shielding concrete. Traditionally coarse aggregates (about 1 cm average size) have been employed in the fabrication of concrete for shielding applications. The advent of nanotechnology, however, has opened up new opportunities to enhance the properties of radiation shielding concrete at nanoscale. Most of the work on this area has been concentrated on the inclusion of nanomaterials to increase the low tensile strength and strain capacities of cement based materials. There have been many recent studies on newly produced nanomaterials such as nanosilica, nanotitanium oxide, nanoiron oxide, carbon nanotubes (CNTs) and graphene oxide (GO) sheets that could be used for concrete reinforcement. Figure 2.3 shows the sizes of typical nanofillers that have the potential to improve the strength and the durability of concrete. Better performance is anticipated by reinforcing cement matrix at nanoscale since their size are closer to that of calcium silicate hydrate (C-S-H) gel [28].

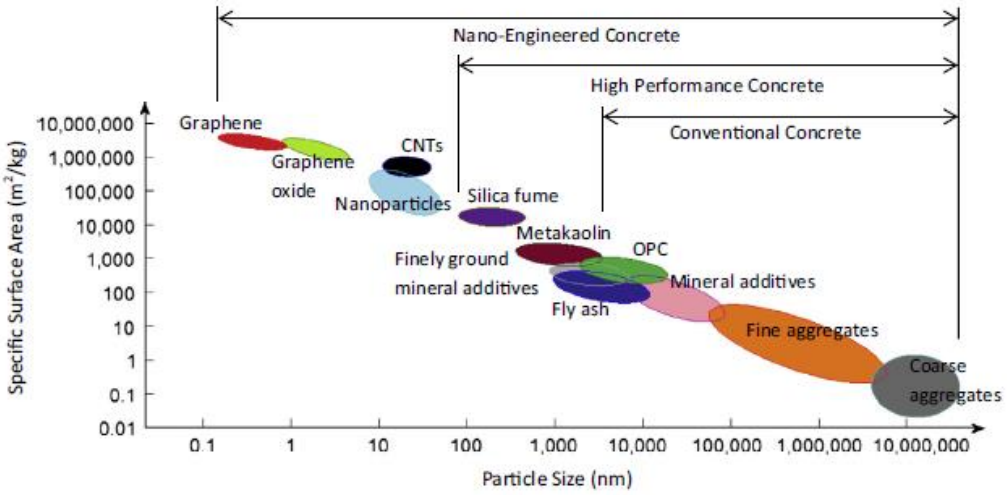

Figure 2.3 Nano fillers for reinforcement of concrete and cementious matrices [28]

The size aggregates could also have an effect on the attenuation properties of concretes. While this topic has been studied to some extent for polymer composites, little is known about the effects of nanofillers in the attenuation properties of concrete. Conventionally, it has been believed that the shielding capacity of a giving material is almost independent of its microstructure, but mainly determined by factors such as the type and energy of radiation, the elemental composition and the density of the material. Yet, recent work has shown improvement of the attenuation capability of concrete with nanofillers compared to their microsized counterparts[29-30]. Since there are different opinions upon how the nano effect can improve the radiation shielding properties, it is prudent to conduct further investigations to look into these effects, if only to discount them as unimportant.

Besides the addition of aggregates admixtures, the attenuation properties of concrete are also determined by the amount of atomic hydrogen present in the attenuator. As mentioned earlier, hydrogen is one of the best candidates for neutron shielding because it can efficiently slow down the fast neutrons through elastic scattering. Several works have studied the variation of the attenuation properties in concretes with addition of different hydrogen sources. Belyakov and coworkers[31] reported the shielding characteristics of polymer based concretes such as furfurylidene acetone polymer. Gunduz and Usanmaz [32] studied shielding properties of polymer impregnated concrete

with boron frit as aggregate. Azharul Islam *et al* [33] investigated the shielding properties of polyethylene (PE), lead (Pb), ordinary concrete (OC), heavy concrete (HC), and their multi layer PE+OC, PE+HC and PE+Pb. Karitha[34] et al studied the effect of water cement/ratio on shielding performance of concrete. Shanin *et al*[35] studied the effect of water to cement ratio, curing conditions, dosage of cement and air entraining agent on the gamma radiation shielding performance. As expected, all these works reported improvement on neutron shielding performances when concrete was loaded with sources containing sufficient hydrogen nuclei.

2.4. COMPUTATIONAL METHODS

In the last few decades, several computational methods such as the Monte Carlo algorithm have become an indispensible tool to design radiation shielding concretes for nuclear applications. The use of these techniques allows not only to perform efficient and accurate radiation calculations in complex 3D geometries, but they also help to find the optimum chemical composition of concrete that gives the most suitable attenuation, mechanical and physicochemical properties for a given application. Some of the advantages of using computational techniques for designing RSC are: 1) allows for sensitivity analysis and optimization for real system without need to operate the real system, 2) there is better control over experimental conditions than the real system; 3) it is possible to evaluate the system on a slower or faster time scale than the real system.

The Monte Carlo algorithm is used in particle physics to solve the Boltzmann transport equation that models the propagation of radiation through matter. The transport equation cannot be solved analytically for many practical situations; therefore, it is necessary to use numerical techniques such as the Monte Carlo method to obtain realistic solutions of the transport equation in 3D complex geometries. Monte Carlo method consists of simulating a finite number of particles histories through the use of a pseudo random number generator [36]. In each particle history random numbers are generated and used to sample appropriate probability distributions for particle/photon initial energy, direction of motion, step length, interacting nucleus, type of interaction, new direction, etc. By tracking each particle history it is possible to calculate the expectation or mean value $\bar{x}$ of some quantities such as the flux, current, escape probability, or any number of other quantities. Since this method is essentially based on statistical concepts, the answer

it gives is not unique; rather it is an estimate which should lie within some confidence interval about the "true" answer. The uncertainty associated with the result decreases with increasing number of histories.

Several authors have investigated the attenuation properties of concretes using Monte Carlo simulations. The majority of the published work has examined the gamma ray attenuation coefficients for concretes with iron , lead [19], barium [37] and other mineral admixtures[38]. Gencel *et al* [13] carried out numerical calculations using the Monte Carlo N-Particle code (MCNP) to determine the gamma shielding characteristics of concretes having different hematite proportions. Computational investigations of neutron shielding have also been reported for several concrete compositions with boron and polymers additions [39-40]. Sariyer and coworkers [41] studied the neutron attenuation properties of concrete modified with ferro boron and boron carbide using FLUKA Monte Carlo simulation code. Piotrowski and collaborators [42] study the importance of atomic composition and moisture content of cement based composites in neutron shielding using MCNP. Agosteo *et a l*[43] evaluated the shielding capabilities of concrete for hadron-therapy accelerators through Monte Carlo simulation with FLUKA code. All these simulation works have been validated with experimental measurements showing good agreement between the two techniques.

PAPER

I. MECHANICAL BEHAVIOR AND GAMMA RAY ATTENUATION PROPERTIES OF MAGNETITE-CEMENT COMPOSITES

Henry A. Colorado[a], Raul Florez[b], Carlos Castano-Giraldo[b], Ayodeji Alajo[b]

[a] Composites Laboratory, Universidad de Antioquia (UdeA), Calle 70 No. 52-21, Medellin, Colombia.

[b] Nuclear Engineering, Missouri University of Science and Technology, 301 W. 14th St., Rolla, MO 65409, USA

ABSTRACT

This paper concerns about the mechanical, structural and gamma ray attenuation properties of eight magnetite-cement composites for potential applications in nuclear radiation shielding. Scanning electron microscopy and x-ray diffraction were used to investigate the microstructure of the samples. Compression and density test were done over all samples. Gamma ray transmission experiments were conducted at 0.662 MeV to determine the mass attenuation coefficient of the pastes. The results of the transmission experiments were compared with those obtained from Monte Carlo N-Particle (MCNP) simulations and XCOM database. Good agreement was found among experimental, simulation and theoretical data. Results show that fine magnetite powder is an effective aggregate for enhancing the mechanical properties of WOPC pastes; however, its effect on the gamma ray attenuation properties is insignificant at the evaluated energy. Moreover, the addition of magnetite reduces the density of the cement pastes making them unsuitable for gamma ray shielding.

Keywords: Magnetite, Porland Cement, SEM, XRD, shielding, MCNP, XCOM

1. INTRODUCTION

Gamma and X-rays are produced in a variety of medical, industrial and research facilities. As a general rule, levels of exposure to these kinds of radiations should be minimized to prevent the potential hazards that they can pose for human beings. One of the main methods for minimizing exposure to ionizing radiation is shielding. For this reason, the development of new materials with excellent shielding, chemical, physical and mechanical properties, is of interest to the scientific community.

Among the many shielding materials studied, cementitious matrices are of particular importance because of their high strength, low cost and convenience in production. They are commonly used as structural materials in constructions where shielding of ionizing radiation is required including Nuclear Power Plants (NPP), geological repositories, hospitals, laboratories, among others. A significant number of experimental and theoretical studies are available on the radiation shielding properties of cement based materials [1-5]. Most research has been devoted to the development of high density concretes for gamma protection [6-8]. Heavy density concretes are usually fabricated mixing cement matrices with high Z admixtures [9-10] and other mineral aggregates such as iron oxides [11-12], silica fume [13], fly ash [14], among others. Similarly, other studies have been concerned with the fabrication of low weight cement based materials which could provide not only good structural properties but also good shielding capability [15].

Magnetite is a naturally occurring iron oxide which has been extensively used in the fabrication of cement based materials for shielding applications. Numerous studies have demonstrated the positive effects of using magnetite for the attenuation, physicochemical and mechanical properties of cement composites [16-19]. Most of the research has focused on the use of magnetite as coarse aggregate; however, the recent work published by Ouda [6] shows that magnetite as a fine aggregate can also enhance the mechanical properties of heavy weight concretes used in shielding applications. Further studies are needed in order to fully understand the role of fine aggregate magnetite on the properties of cement based material, as well as its potential in the fabrication of new light weight shielding materials.

The aim of the present work is to study the effect of the addition of fine magnetite powder on the mechanical, physicochemical and gamma attenuation properties of white ordinary Portland cement (WOPC) pastes. The compressive strength and microstructure of the cement pastes with different rates of magnetite were determined. Additionally, the photon attenuation coefficients for the different composite pastes were also measured experimentally at 0.662 MeV. The obtained experimental data was compared with the theoretical values obtained by XCOM [20].

2. EXPERIMENTAL METHODS AND SIMULATION

2.1. MATERIALS

White ordinary Portland cement (Holcim S.A, Colombia) and commercially available magnetite powder (Ferrominerales Ltd, Colombia) with an average particle size of X µm were used as starting materials in this study. The chemical properties for WOPC and magnetite powder are summarized in Table 2.1.

Table 2.1 Chemical properties of WOPC and magnetite

Chemical Composition	**WOPC**	**Magnetite**
CaO (%)	65.2	3.4
SiO_2 (%)	20.1	2.28
Al_2O_3 (%)	4.28	0.8
MgO (%)	2.9	0.52
Fe_2O_3 (%)	3.02	-
SO_3 (%)	3	-
MnO (%)	-	0.8
Fe_3O_4	-	87.0
LOI	1.5	5.2

2.2. COMPOSITE PROCESSING

Seven types of Fe_3O_4-WOPC composite materials, designated M4, M5, M6, M7, M8, M9 and M10, were prepared. An additional plain WOPC paste, named M1 was also fabricated and was used as a control material. Sample names and compositions are given in Table 2.2. For all mixtures the water-to-cement ratio was kept at 0.4. Each paste was prepared according to the following procedure. Firstly, Fe_3O_4 powder and WOPC were mixed mechanically for 30 min in a X. Subsequently, the powder was mixed with water for 15 min at 60 rpm. The resulting paste was then cast into cylindrical molds with an inner diameter of 20 cm and 30 cm depth. After 24 hours, the hardened cement specimen was demolded and cured in a hermetically closed container over 28 days. All the specimens were allowed to dry in the air for 12 h before they were subjected to mechanical test.

2.3. MECHANICAL TESTING

The compressive strength of the cement pastes was measured according to the standard procedure. Compressive strengths tests were conducted on cubes. To characterize the tensile behavior of each specimen, uniaxial tension tests were performed on the specimens using an Instron Machine 3382. A set of N samples were tested using a crosshead speed of 1mm min^{-1}. During the tests, the loading force and elongation were measured. Two linear variable differential transducers were attached to both sides of the center of the tensile specimen to measure the elongation.

Table 2.2 Composition of the cement samples used in this study

Sample	Powder (g)		Liquid (g)
	WOPC	Fe_3O_4	Water
M1	100	0	40
M4	99	1	39.6
M5	97.5	2.5	39
M6	95	5	38
M7	90	10	36
M8	80	20	32
M9	60	40	24
M10	50	50	20

2.4. STRUCTURAL ANALYSIS

The microstructural properties of magnetite-WOPC composites were evaluated by x-ray diffraction (XRD) and scanning electron microscopy (SEM). XRD measurements were conducted in an X'Pert PRO diffractometer (Cu Kα radiation, λ=1.5406 Å), using 45 kV voltage and scanning between 28° and 58°. SEM Images were acquired using a JEOL JSM 6700R high resolution scanning electron microscope in high vacuum mode. The operation voltage was 20 kV and images were taken at five different magnifications (500x, 1000x, 2000x, 5000x and 10000x). All samples analyzed by SEM were subjected to a preparation procedure to get a flat surface with uniform analysis condition across the region of interest. The preparation procedure required the samples to be dehydrated in a furnace at 30 ℃ for 24 hours. The samples were then cracked to expose the microstructure. Thereafter, samples were sputtered in a Hummer 6.2 system (15 mA AC for 30 sec) creating approximately a 1nm thick film of Au.

2.5. GAMMA RAY ATTENUATION

The linear attenuation coefficients (μ, cm^{-1}) of the samples were measured by gamma transmission experiments in narrow beam geometry conditions. Figure 2.1 shows the experimental arrangement layout and the measuring system used in the present work. The photon transmission values were measured using a detection system consisting of a scintillation sodium iodide NaI(Tl) detector (Ortec 3M3/3-X), a photomultiplier base tube with preamplifier (Ortec 276), a high voltage supply (Ortec 556), a amplifier (Ortec 672) and a multichannel analyzer (Ortec Easy MCA). Gamma spectra were obtained with the acquisition software Maestro. A Cs^{137} (662 keV) source was used. The source was shielded by pin hole lead collimator to obtained narrow beam conditions. Each experiment was counted for 45 minutes. The linear attenuation coefficient (μ, cm^{-1}) were the calculated using the Lambert-Beer's equation:

$$\mu(E) = -\frac{1}{x} ln\left(\frac{I_x(E)}{I_0(E)}\right) \quad (1)$$

Where x is the sample thickness, $I_x$and I_0 are the incident and transmitted beam intensities respectively. The incident intensity was determined without a shielding sample present.

The half value layer (HVL) and the tenth value layer (TVL) for each pastes were also calculates. HVL and TVL are the thickness of a given material needed to reduce the intensity of the incident radiation to 50% and 90% respectively. They are calculated as follows:

$$HVL = \frac{0.693}{\mu}, \qquad TVL = \frac{2.303}{\mu} \quad (2)$$

The overall error in the experimental measurements was calculated using error propagation rules. The error is due to the evaluation of peak areas, sample thickness measurement, density measurements and counting statistics.

2.6. XCOM CALCULATIONS

Theoretical values of the mass attenuation coefficient for the samples were also calculated using the program XCOM[20]. This is a photon cross section database compiled by the National Institute of Standards and Technology of the United States of

America (NIST). XCOM provides the total cross section as well as the partial cross section for the following processes: incoherent scattering, coherent scattering, photoelectric absorption, and pair production in the field of the atomic nucleus and in the field of atomic electrons. Table 2.3 shows the quantum theoretical models used to obtain the cross sections for the aforementioned processes. The data concerns elements with atomic number up to 100 and photon energies from 1 keV to 1GeV. Cross sections for compounds are also determined by XCOM using a weighted mixture rule for the atomic constituents. In this case, the chemical effect, molecular bonding and crystal structure of the chemical compounds are neglected by the mixture rule used by XCOM[20].

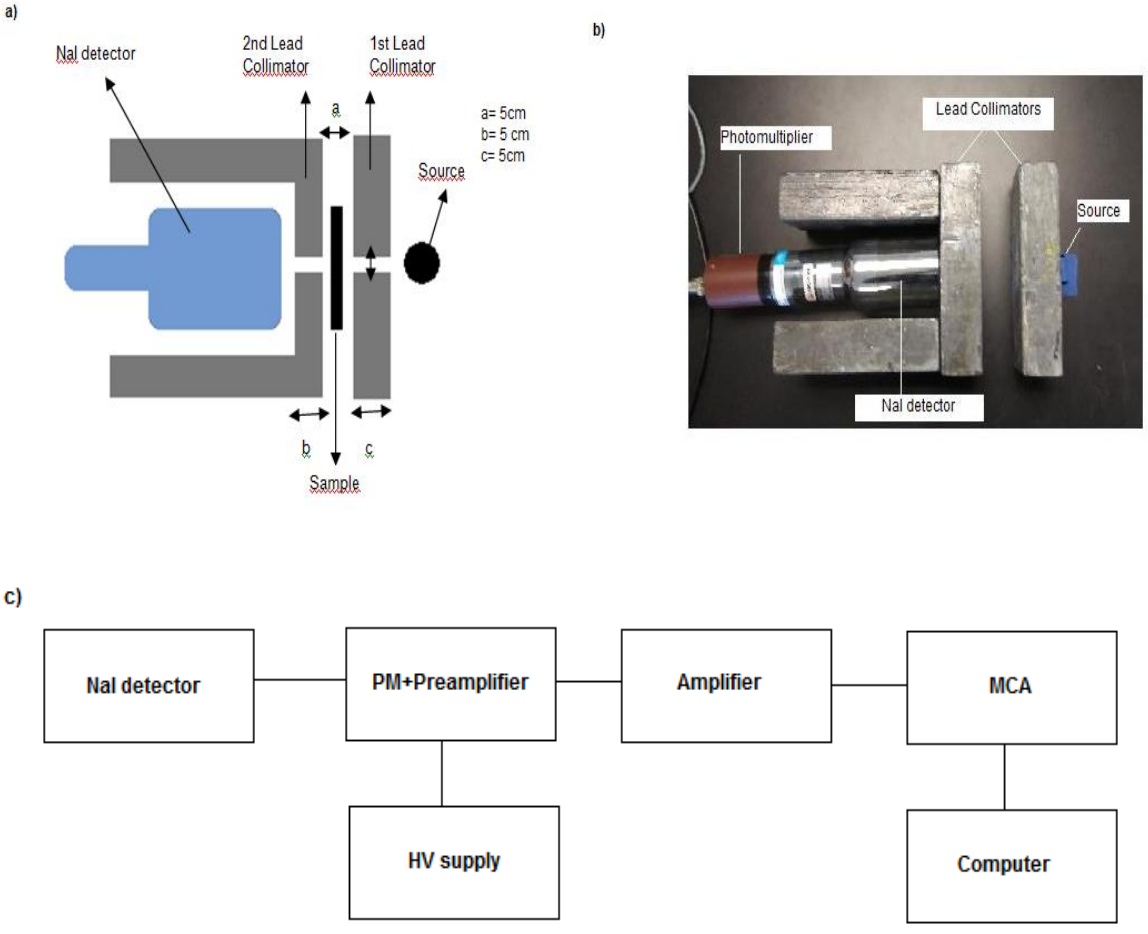

Figure 2.1 a) Narrow beam geometrical set up, b) Picture of the experimental setup, c) Layout of the radiation counting system

Table 2.3 Theoretical models used in XCOM database [20]

Interaction Mechanism	**Models**
Incoherent scattering	Nishima-Klein equation and non relativistic Hartree-Fock incoherent scattering functions.
Coherent scattering	Thomson formula and relativistic Hartree-Fock atomic form factors.
Photoelectric	$\leq$ 1.5 MeV Scofield's equation. $>$ 1.5 MeV Semiempirical equation calculated by Pratt.
Pair-production	Bethe-Heitler theory.

XCOM was also used to calculate the equivalent atomic number Z_{eq} of the cement. This is a single parameter used to describe the properties of the composites in terms of the equivalent elements and identify the predominant attenuation mechanism at different energy regions. Z_{eq} can be estimated from the ratio of the Compton partial mass attenuation coefficient relative to the total mass attenuation coefficient at a specific photon energy, using the following equation:

$$Z_{eq} = \frac{Z_1(\log R_2 - \log R) + Z_2(\log R - \log R_1)}{\log R_2 - \log R_1} \quad (3)$$

Where Z_1 and Z_2 are the atomic numbers of elements corresponding to $\left(\frac{\mu_{comp}}{\mu_{total}}\right)$ ratios R_1 and R_2 respectively, and R $\left(\frac{\mu_{comp}}{\mu_{total}}\right)$ is the ratio for the selected material at a particular energy, which lies between R_1 and R_2.

2.7. MCNP SIMULATIONS

A Monte Carlo code was developed to estimate the attenuation parameters of the cement samples. Radiation transport calculations were done using the Monte Carlo N-Particle (MCNP) code, version 6.1 [21] . This software is widely used in radiation physics for neutron, photon, electron, and coupled neutron/photon/electron transport calculations. In this work, the calculations were performed only in the photon transport mode. Attenuation of photons is calculated by simulating all relevant physical processes and interactions before and after inserting the investigated sample. The simulations assumed that the samples do not have any cracks and the chemical composition is

homogeneous throughout all the volume. Tally F2 was used to obtain the average surface flux at the detector location. All simulations were performed with 100000 histories and the tally results passed all statistical checks and had relative errors less than 1%.

2.7.1. Geometry. For modeling purposes, the geometry of the transmission experiment presented in section 2.5 was simplified as shown in Figure 2.2. The simulated geometry consists of two identical lead bricks with hole in the center which are used as collimators for gamma rays. The two lead bricks are aligned between source and detector and separated by 5cm from each other. The simulated samples consist of cylinders with the same dimensions as the samples used for transmission experiments. The photon weight factor is 1 in all cells and zero in the cutoff region (outside the boundary surface of the problem).

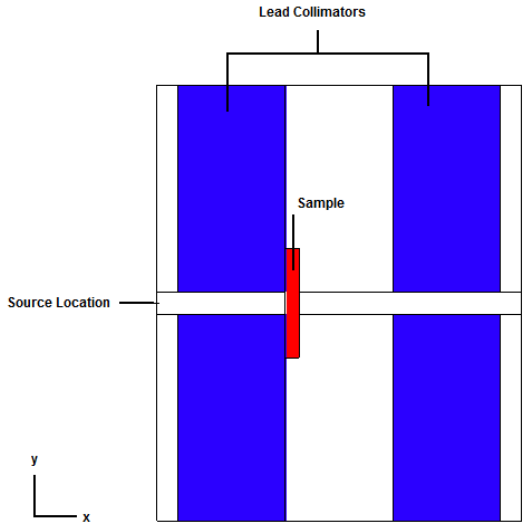

Figure 2.2 Simulation setup for MCNP calculations

2.7.2. Gamma Source and Detector. The radiation source was modeled as a isotropic, monoenergetic point source for the selected gamma ray energy of 0.662 MeV. The source is located at 0.5 cm away from the entry plane of the first lead collimator whereas the detector (F2 tally) was located at the exit plane of the second lead collimator.

2.7.3. Material Specification. The elemental composition of the samples used in MCNP simulations was determined from the mix proportions and oxide composition of the starting materials given in section 2.1. The corrected composition for each sample

was calculated following the procedure described by Piotroski *et al* [22]. Table 2.4 summarizes the elemental composition of each sample used for MCNP simulations.

Table 2.4 Elemental Composition of samples used for MCNP simulations

Sample	Density (g/cm^3)	Element Weight (%)								
		H	Si	O	Al	Fe	Ca	Mg	S	Mn
M1	1.80	3.17	6.81	50.90	1.64	1.53	33.80	1.27	0.87	-
M5	1.88	3.12	6.69	50.48	1.61	2.80	33.19	1.25	0.86	0.01
M6	1.84	3.06	6.57	50.06	1.58	4.10	32.57	1.22	0.84	0.02
M7	1.70	2.94	6.31	49.19	1.52	6.74	31.31	1.17	0.81	0.05
M8	1.75	2.69	5.78	47.38	1.39	12.26	28.68	1.08	0.74	0.10
M9	1.60	2.15	4.62	43.40	1.11	24.37	22.89	0.86	0.59	0.21
M10	1.40	1.85	3.98	41.22	0.96	31.04	19.71	0.74	0.51	0.27

3. RESULTS AND DISCUSSION

3.1. COMPRESSIVE STRENGTH

Figure 3.1 shows the variations in the compressive strengths of the hardened WOPC pastes modified with different ratios of magnetite at 28 days of curing. For pastes made of mixes M5, M6, M7 and M8, the compressive strength values were found to be higher than the one obtained for the control cement sample M1. An overall analysis of Figure 3.1 shows that the correlation between the compressive strength and magnetite concentration is complex, but it tends to have a maximum enhancement about 10 wt% of magnetite, with strength decreasing again at higher values. This behavior is also observed in the stress strain curves of next section. Hydration tests are needed to gain additional understanding into the different competing mechanism responsible for this behavior.

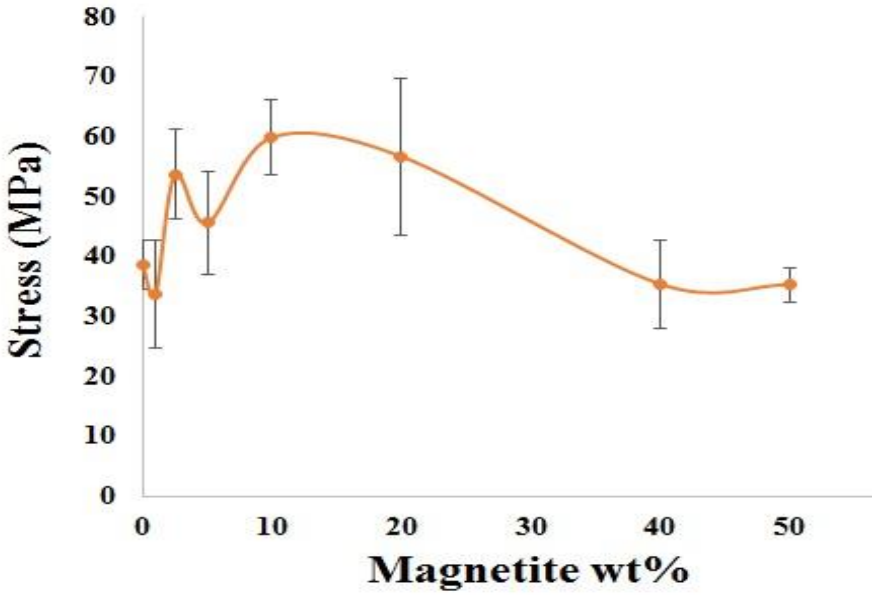

Figure 3.1 Effect of magnetite on the compressive strength of magnetite- WOPC composites

Typical stress-strain curves for the control and the composite specimens are presented in Figure 3.2. In order to understand the effect of magnetite addition to the stress-strain behavior of the samples, both the pre-peak and the post-peak regions are analyzed separately. Firstly, one of the most notorious effects in the pre-peak zone is the

change in the strength of the samples due to magnetite addition. Specimens M4, M5, M6, M7 and M8 show an increment in the peak stress relative to the plain sample, whereas specimens M9 and M10 a reduction in the peak strength is observed. It is also worth noticing that all the samples with magnetite show an increase in the strain corresponding to peak stress which suggests that the initiation of microcracks propagation is delayed by the presence of magnetite. As far as the post-peak zone is concerned, the curves show that cementious matrices M1, M4, M8 and M10 have a sharp descending branch which is characteristic of brittle materials. On the other hand, samples M5, M6, M7 and M9 exhibit a more slowly and longer descending branch; thus, these specimens are not only more ductile but they are also more tough than the control sample.

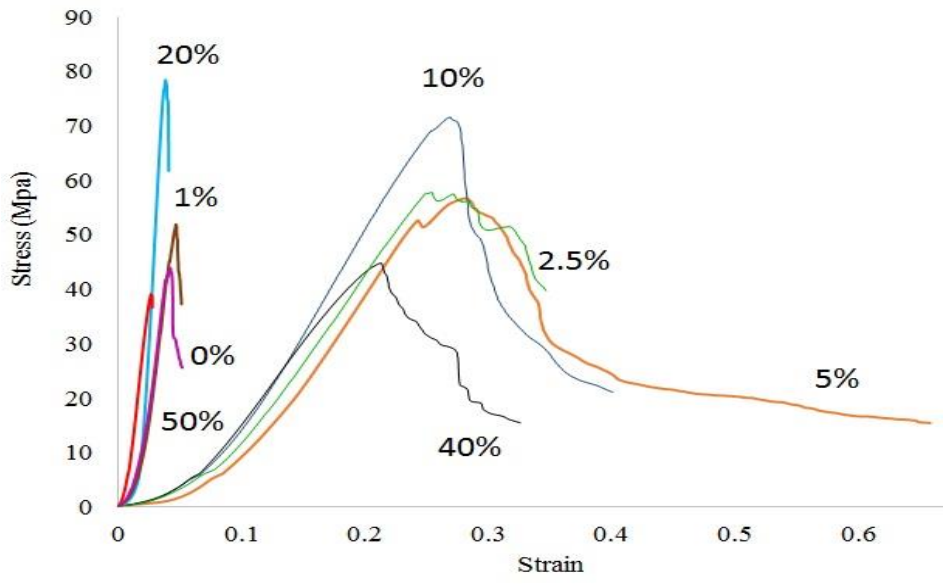

Figure 3.2 Typical stress-strain curves for the cement-magnetite composites

3.2. DENSITY

The density values for the fabricated pastes are shown in Figure. 3.3. In general, it is observed that the addition of magnetite decreases the density of the specimens; however, it is not easy to establish a correlation between these two variables because the behavior is complex.

3.3. MICROSTRUCTURE

SEM images of the control cement paste and the composites with 1%, 2.5%, 5%, 10%, 20%, 40% and 50% magnetite are shown in Figure 3.4. The improvement on the mechanical and physical properties of the samples reinforced with magnetite can be elucidated through the microstructural characteristics observed in the micrographs. For the cement pastes containing 2.5%, 10% and 20% magnetite, the SEM images reveal that there is a uniform microstructure with good distribution of magnetite particles throughout the cementitious matrix. For this reason, and due to the filling effect of the magnetite particles, higher values of compressive strength and density are obtained for these specimens as compared to those obtained for the plain cement sample. On the other hand, the SEM micrographs of the specimens with 40% and 50% magnetite show a relative less homogeneous microstructure with some agglomerated magnetite particles. This microstructural heterogeneity explains why the addition of magnetite beyond 20 wt% leads to a reduction of both compressive strength and density.

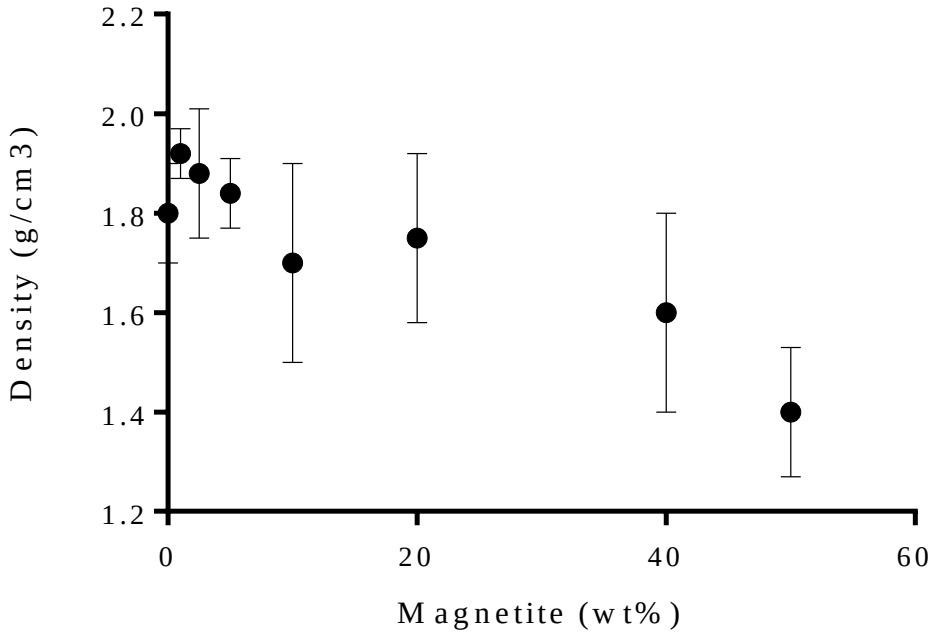

Figure 3.3 Bulk density of the fabricated paste as a function of the magnetite concentration

3.4. XRD

Figure 3.5 shows the XRD patters for the WOPC with magnetite samples fabricated. Results show that magnetite particles did not interact much to form new radical phases more than the normal one that appear in cement. As expected, magnetite contents increase in samples with the magnetite loading. This is in some way a good result since we do not expect to decompose magnetite and preserve its mechanical and shielding properties.

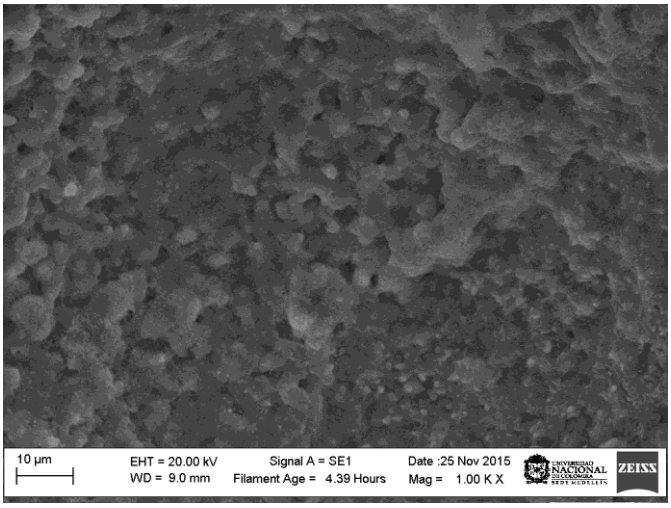

Figure 3.4 SEM micrographs of the studied samples

3.5. GAMMA RAY ATTENUATION

Figure 3.6 shows the mass attenuation coefficients (MCA) for the investigated composites obtained from the experimental measurements at 0.662 MeV. The results suggest that the addition of magnetite does not modify the attenuation properties of cement pastes significantly. This can be attributed to the low contribution of the photoelectric absorption and pair production attenuation mechanisms at this range of energy. The experimental HVL and TVL for the WOPC-magnetite composites are plotted in Figure 3.7. Even though the variation in the values for the different composites is small, the trend in the plot shows that sample with 10 wt% of magnetite shows the minimum HVL and TVL indicating that this composition is slightly advantageous from a radiological standpoint.

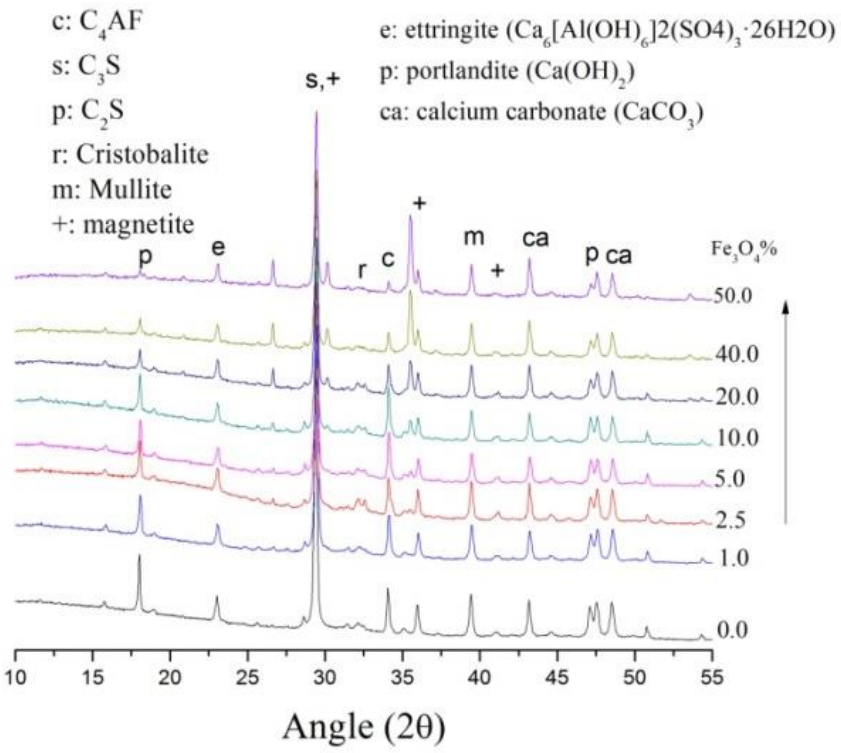

Figure 3.5 XRD patterns for white ordinary Portland cement paste with magnetite

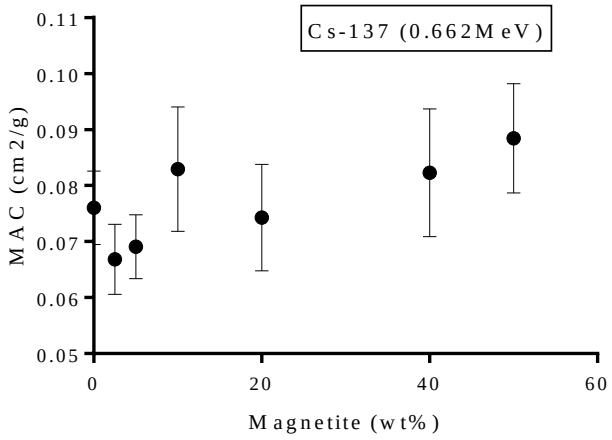

Figure 3.6 Total mass attenuation coefficient (cm2/g) of gamma rays at 0.662 MeV for the WOPC-Magnetite composites

Table 3.1 compares the different values of MCAs obtained from experiments, MCNP simulations and XCOM. The data is also plotted in Figure 3.8. In general, there is satisfactory agreement between the experimental, simulation and theoretical values. Differences between experimental and theoretical results can be attributed to deviation from the narrow beam geometry in the source detector arrangement.

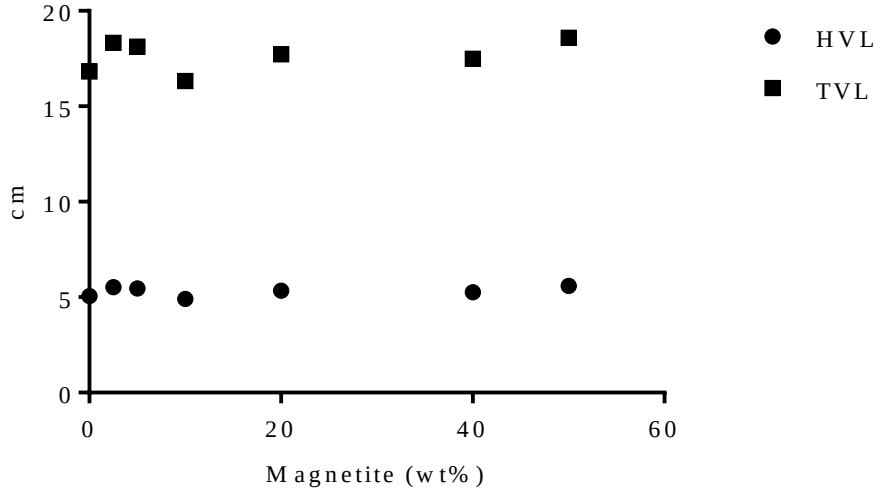

Figure 3.7 Experimental HVL and TVL at 0.662 MeV for the WOPC-Magnetite composites

Table 3.1 Mass attenuation coefficient of the studies samples obtained from experimental measurements, MCNP simulations and XCOM database

Sample (Magnetite wt%)	Experimental	% SD	MCNP	%RPD	XCOM	%RPD
M1 (0%)	0.07601	8.5%	0.07032	0.077	0.07976	0.048
M5 (2.5%)	0.06683	9.3%	0.06910	0.033	0.07930	0.171
M6 (5.0%)	0.06906	8.2%	0.06544	0.053	0.07920	0.137
M7 (10%)	0.08293	13%	0.07113	0.153	0.07898	0.049
M8 (20%)	0.07426	12%	0.06739	0.096	0.07854	0.056
M9 (40%)	0.08229	13%	0.07154	0.139	0.07757	0.059
M10 (50%)	0.08843	11%	0.08459	0.044	0.07703	0.138

Table 3.2 shows the effective atomic number (Z_{eff}) for each sample calculated from XCOM data. As shown in Figure 3.9, at 0.662 MeV the predominant interaction of gamma rays in the samples is Compton scattering. The compositional effect on the attenuation properties of the samples is reduced when Compton scattering is the dominant attenuation mechanism. For this reason, differences in the chemical composition of the fabricated samples can produce only minimal changes on the attenuation properties in the Compton dominated region.

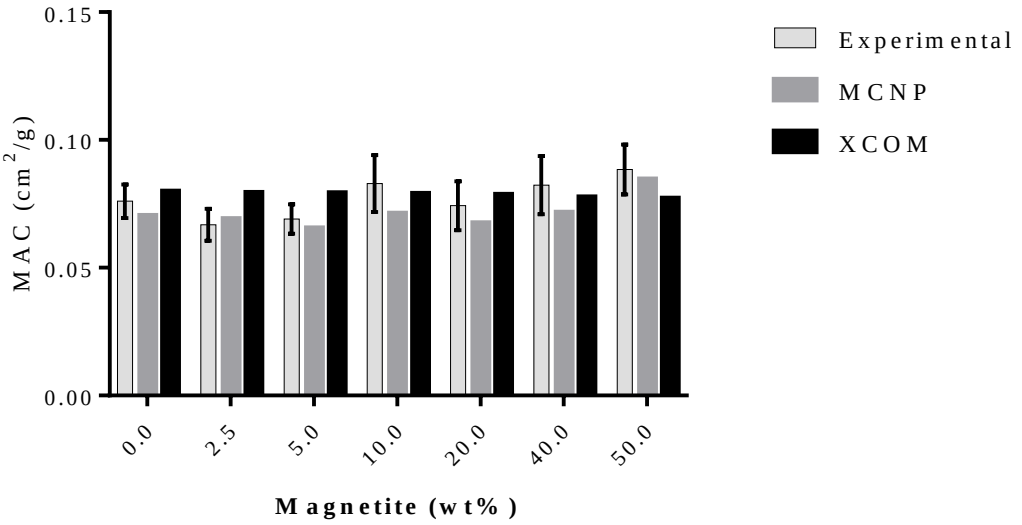

Figure 3.8 Mass attenuation coefficients for WOPC-magnetite pastes calculated from experimental data, MCNP simulations and XCOM database

Table 3.2 Effective atomic number Zeff for the studied samples

Sample	Magnetite (wt%)	Z_{eff}
M1	0	21.93
M5	2.5	17.06
M6	5	17.03
M7	10	17.01
M8	20	17.63
M9	40	18.78
M10	50	20.01

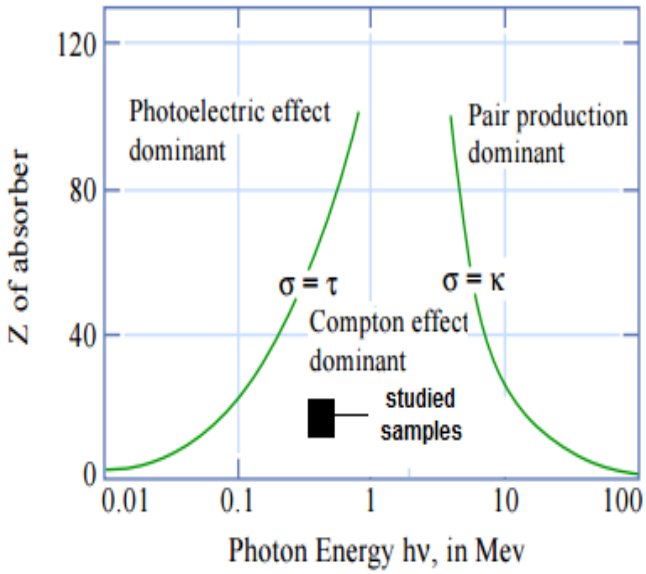

Figure 3.9 Relative importance of the photon attenuation mechanisms in the studied samples

4. CONCLUSIONS

The present work analyzed the microstructural, mechanical and gamma attenuation properties of various composites made of white ordinary Portland cement and magnetite. On the basis of the previous experimental findings, the following conclusions can be derived:

- The addition of magnetite affects the mechanical properties of the cement pastes. The hardened pastes made of magnetite-WOPC mixture with 2.5%, 5%, 10% and 20% by weight of magnetite showed higher compressive strength values than the plain WOPC paste. The highest value of compressive strength was obtained by substitution of WOPC with 10 wt% of magnetite. Conversely, substitution of WOPC with 1%, 40% and 50% by weight of magnetite reduce the compressive strength of the pastes with respect to the plain WOPC paste.
- The addition of magnetite to WOPC pastes also affects the stress-strain response of the samples. On the one hand, composites with 1% and 20% by weight of magnetite exhibited the same kind of brittle behavior obtained for the plain WOPC paste; although, these pastes showed a higher peak stress with respect to the control sample. On the other hand, a more ductile behavior was observed in composites prepared with magnetite additions of 2.5%, 5%, 10%, and 40%. For all these samples, the peak stress and the strain corresponding to peak stress were enhanced with respect to the plain WOPC control sample. Further improvements in toughness are also achieved for the samples with ductile behavior.
- Analysis of cement-magnetite composites microstructures from SEM images shows that the samples with improved mechanical properties have a homogeneous microstructure with good dispersion of the magnetite particles inside the cement matrix. On the contrary, the samples with poor mechanical performance have a heterogeneous microstructure with some agglomeration of magnetite particles which leads to lower values of compressive and tensile strength.
- Gamma ray attenuation measurements demonstrate that the addition of magnetite has little effect on the attenuation properties of the composite at 0.662 MeV. At this energy, the predominant attenuation mechanism in the samples is Compton scattering;

therefore, the compositional effect upon the attenuation characteristics of the samples is small and the differences in the attenuation properties among the fabricated samples are small too.

- From the calculation and the validation of the experiment performed it is clear that the Monte Carlo method is a feasible numerical technique to predict the attenuation properties of magnetite-WOPC composites. Both experimental and simulation results show good agreement with small differences which are probably attributable to the difference between difference between the simulated and real composition of the cement pastes.

REFERENCES

[1] E. S. A. Waly and M. A. Bourham, "Comparative study of different concrete composition as gamma-ray shielding materials," *Ann. Nucl. Energy*, vol. 85, pp. 306–310, 2015.

[2] B. Oto, N. Yildiz, T. Korkut, and E. Kavaz, "Neutron shielding qualities and gamma ray buildup factors of concretes containing limonite ore," *Nucl. Eng. Des.*, vol. 293, pp. 166–175, 2015.

[3] I. Akkurt, K. Günoglu, C. Basyigit, S. Kilincarslan, and A. Akkas, "Cement paste as a radiation shielding material," *Acta Phys. Pol. A*, vol. 123, no. 2, pp. 341–342, 2013.

[4] C. Ipbüker, H. Nulk, V. Gulik, A. Biland, and A. Henry, "Radiation shielding properties of a novel cement – basalt mixture for nuclear energy applications," *Nucl. Eng. Des.*, vol. 284, pp. 27–37, 2015.

[5] A. Yadollahi, E. Nazemi, A. Zolfaghari, and A. M. Ajorloo, "Application of artificial neural network for predicting the optimal mixture of radiation shielding concrete," *Prog. Nucl. Energy*, vol. 89, pp. 69–77, 2016.

[6] A. S. Ouda, "Development of high-performance heavy density concrete using different aggregates for gamma-ray shielding," *Prog. Nucl. Energy*, vol. 79, pp. 48–55, 2015.

[7] I. Akkurt, H. Akyildirim, B. Mavi, S. Kilincarslan, and C. Basyigit, "Gamma-ray shielding properties of concrete including barite at different energies," *Prog. Nucl. Energy*, vol. 52, no. 7, pp. 620–623, 2010.

[8] D. Jóźwiak-Niedźwiedzka, K. Gibas, A. M. Brandt, M. A. Glinicki, M. Dąbrowski, and P. Denis, "Mineral Composition of Heavy Aggregates for Nuclear Shielding Concrete in Relation to Alkali-silica Reaction," *Procedia Eng.*, vol. 108, pp. 162–169, 2015.

[9] D. Rezaei-Ochbelagh and S. Azimkhani, "Investigation of gamma-ray shielding properties of concrete containing different percentages of lead," *Appl. Radiat. Isot.*, vol. 70, no. 10, pp. 2282–2286, 2012.

[10] H. E. Hassan, H. M. Badran, A. Aydarous, and T. Sharshar, "Studying the effect of nano lead compounds additives on the concrete shielding properties for ??-rays," *Nucl. Instruments Methods Phys. Res. Sect. B Beam Interact. with Mater. Atoms*, vol. 360, pp. 81–89, 2015.

[11] O. Gencel, A. Bozkurt, E. Kam, and T. Korkut, "Determination and calculation of gamma and neutron shielding characteristics of concretes containing different hematite proportions," *Ann. Nucl. Energy*, vol. 38, no. 12, pp. 2719–2723, 2011.

[12] S. Sharifi, R. Bagheri, and S. P. Shirmardi, “Comparison of shielding properties for ordinary, barite, serpentine and steel-magnetite concretes using MCNP-4C code and available experimental results,” *Ann. Nucl. Energy*, vol. 53, pp. 529–534, 2013.

[13] S. Akbulut, A. Sehhatigdiri, H. Eroglu, and S. ??elik, “A research on the radiation shielding effects of clay, silica fume and cement samples,” *Radiat. Phys. Chem.*, vol. 117, pp. 88–92, 2015.

[14] K. Singh, S. Singh, and G. Singh, “Effect of Flyash Addition on Mechanical and Gamma Radiation Shielding Properties of Concrete,” vol. 2014, 2014.

[15] I. Akkurt, H. Akyildirim, B. Mavi, S. Kilincarslan, and C. Basyigit, “Radiation shielding of concrete containing zeolite,” *Radiat. Meas.*, vol. 45, no. 7, pp. 827–830, 2010.

[16] E. Horszczaruk, P. Sikora, and P. Zaporowski, “Mechanical properties of shielding concrete with magnetite aggregate subjected to high temperature,” *Procedia Eng.*, vol. 108, pp. 39–46, 2015.

[17] B. Oto, N. Yıldız, F. Akdemir, and E. Kavaz, “Investigation of gamma radiation shielding properties of various ores,” *Prog. Nucl. Energy*, vol. 85, pp. 391–403, 2015.

[18] B. Oto and A. Gür, “Gamma-ray shielding of concretes including magnetite in different rate,” *Int. J. Phys. Sci.*, vol. 8, no. 8, pp. 310–314, 2013.

[19] M. A. El-Sarraf and A. El-Sayed Abdo, “Influence of magnetite, ilmenite and boron carbide on radiation attenuation of polyester composites,” *Radiat. Phys. Chem.*, vol. 88, pp. 21–26, 2013.

[20] K. Berger, M.J., Hubbell, J.H., Seltzer, S.M., Chang, J., Coursey, J.S, Sukumar, R., Zucker, D.S., Olsen, “XCOM: photon cross sections database.” NIST standard reference database (XGAM), 2010.

[21] “MCNP—A General Monte Carlo N-Particle Transport Code-Version 6.1.” Los Alamos National Laboratory, 2013.

[22] T. Piotrowski, M. Mazgaj, A. Żak, and J. Skubalski, “Importance of Atomic Composition and Moisture Content of Cement based Composites in Neutron Radiation Shielding,” *Procedia Eng.*, vol. 108, pp. 616–623, 2015.

II. NEUTRON ATTENUATION PROPERTIES OF CEMENT PASTES MODIFIED WITH SAMARIUM OXIDE (SM_2O_3)

Raul Florez[a], Henry A. Colorado[b], Carlos Castano-Giraldo[a], Ayodeji Alajo[a]

[a] Nuclear Engineering, Missouri University of Science and Technology, 301 W. 14th St., Rolla, MO 65409, USA

[b] CompositesLaboratory, Universidad de Antioquia (UdeA), Calle 70 No. 52-21, Medellin, Colombia.

ABSTRACT

This work present research on the neutron shielding properties of white ordinary Portland cement (WOPC) pastes modified with samarium oxide (Sm_2O_3). Five composites with varied content of Sm_2O_3 were prepared in order to evaluate the effect of the additive on the thermal neutron attenuation properties. Neutron transmission experiments were conducted using a PuBe neutron source moderated with light water. Monte Carlo n-Particle (MCNP) simulations were also performed in parallel. Good agreement was found between the experimental and simulation results with some differences attributable to uncertainties in the energy spectrum and chemical composition of the simulated source. Both experimental and simulation results show that samarium oxide is an effective additive to enhance the attenuation properties of WOPC against thermal neutrons. A linear correlation was observed between the effectiveness of the shielding and the concentration of samarium oxide in the paste.

Keywords: Cement pastes, Samarium Oxide, Neutron Shielding, Monte Carlo Simulation.

1. INTRODUCTION

Concrete is a composite material which is extensively used for radiation shielding in facilities such as particles accelerators, hospitals, nuclear power plants and nuclear repositories. Besides their excellent structural properties, the attenuation properties of concrete can be customized according to the specific radiation type, the activity of the source and the radiation dose. This is done by using different additives which modify the radiation shielding capability of concrete without causing detrimental effects on the structural and engineering properties such as compressive strength and workability.

The role of the chemical composition of concrete is particularly important for the effective attenuation of neutrons in nuclear reactors. An extensive body of work has been reported on this area with special interest on the influence of moisture [1-2] and neutron absorbers fillers [3-5] on the neutron attenuation properties in concrete. Traditionally, boron bearing compounds have been used as neutron absorbers in radiation shields [6-8]; however, the attenuation of neutrons with boron compounds leads to the concomitant production of helium bubbles which rapidly deteriorate the mechanical properties of the shielding material [9]. As a result, other mineral admixtures such as rare earth oxides have been also studied as alternative fillers in neutron shields [10-11].

Rare earth elements like gadolinium, europium, samarium and dysprosium are commonly used in the nuclear industry due to its large cross sections for thermal neutrons. Among these rare elements, samarium and its compounds are of special interest for shielding applications in nuclear reactors because of their stability for neutron absorption, relative low cost and natural abundance. Additionally, samarium has a relative high atomic number (Z=62) and hence it can be also used to enhance the attenuation of the gamma radiation emitted by nuclear reactors.

The potential use of samarium in radiation shielding concretes requires further investigation in order to find the optimal mixture with the desired structural and shielding characteristics. In the present work, the effect of samarium oxide on the neutron shielding properties of cement pastes has been investigated. The macroscopic cross sections of cement pastes with varied content of samarium oxide were evaluated using both irradiation measurements and Monte-Carlo calculations.

2. EXPERIMENTAL METHODS

2.1. MATERIALS AND SAMPLE PREPARATION

The samples analyzed in this study were prepared using White ordinary Portland cement (WOPC) supplied by Holcim S.A. Colombia and Samarium (III) Oxide (Sm_2O_3) provided by Alfa Aesar. Table 2.1 shows the chemical composition of the starting powder determined by XRF. Five cement pastes with different loading of samarium oxide were fabricated by mixing water and binder (WOPC+ Sm_2O_3) in a mechanical stirrer for 30 minutes. For all samples the water-to-cement mass ratio (*w/c*) was kept constant at 0.4. After mixing, the pastes were cast into cylindrical moldes and cured in a container hermetically closed to air contact for 28 days. Thereafter, the pastes were demolded and labeled as S0, S1, S5, S10 and S20 with the number representing the mass percentage of samarium oxide replacing cement. Table 2.1 summarizes the composition of the cement samples used in this study.

Table 2.1 Chemical composition of the WOPC cement and Samarium Oxide

Material	Chemical Composition (wt %)
Cement	SiO_2 (20.1), Al_2O_3 (4.28), Fe_2O_3 (3.02), CaO (65.2), MgO (2.9), SO_3 (3.0), Residue (1.5)
Samarium Oxide	Sm_2O_3 (99.9), Total Rare Earth Impurities (0.001 max.)

Table 2.2 Composition of the cement samples used in this study

Sample	Binder (g)		Liquid (g)
	Cement	Sm_2O_3	Water
S0	100	0	40
S1	99	1	39.6
S5	95	5	38
S10	90	10	36
S20	80	20	32

Density test were conducted over all samples fabricated by measuring the weight and cylinder dimensions. Every composition was measured on five samples.

2.2. ATTENUATION EXPERIMENTS

A schematic of the experimental setup used for the neutron transmission measurements and its geometric details are shown in Figure 2.1. The measurements were performed using the thermal neutrons produced by thermalization of the fast neutrons emitted by a PuBe source submerged in light water. The beam of thermal neutrons was extracted using a paraffin collimator in one side of the water container. The counting time was 20 minutes and the neutrons were counted using a Helium-3 proportional neutron detector (0.5NH1/1K Canberra). For all the measurements, the PuBe source was located 17 cm away from the paraffin collimator as indicated in Fig 1(c).

The macroscopic cross section ($\sum, cm^{-1}$) for each sample was calculated using the Lambert-Beer's equation:

$$\sum(E) = -\frac{1}{x} ln\left(\frac{I_x(E)}{I_0(E)}\right) \quad (1)$$

where x is the thickness of the sample, I_x and I_0 are the incident and transmitted beam intensities respectively. The incident intensity was measured without a shielding sample present.

2.3. MNCP SIMULATION

Numerical simulations were performed to compare, verify and validate the accuracy of the experimental results. The simulations were conducted using Monte Carlo N-Particle Transport Code version 6 (MCNP6) developed at the Los Alamos National Laboratory [12]. MCNP6 is a transport code used for modeling the interaction of radiation with matter. In this study, all simulations were performed with 10^8 histories to get fail statistical properties. The error of the simulated results was less than 0.5% in all cases. This error does not include the uncertainties due to material composition, geometry and source definition. No variance reduction techniques were applied.

2.3.1. Geometry and Material Specification. Figure. 2.2 shows the geometrical model used in MCNP simulations. Apart from the He-3 detector, all components of the experimental arrangement were simulated with the same dimensions of the experimental setup described in section 2.2. The geometry of the He-3 neutron detector was simplified

to a small cylinder with dimensions 1 cm x 1 cm. This volume corresponds to the active volume of the neutron detector used in this study.

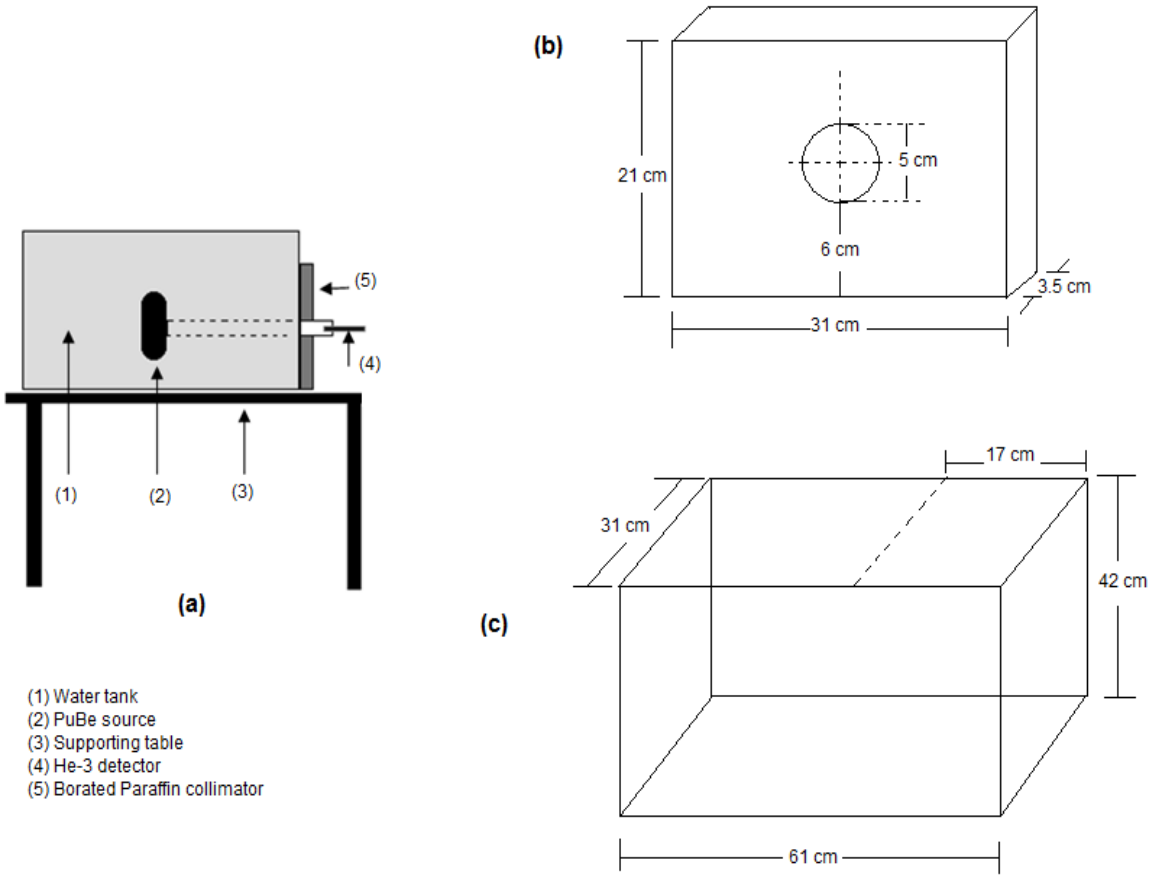

Figure 2.1 (a) Experimental set-up for neutron transmission measurements; (b) paraffin block used as collimator and (c) water tank indicating the source location

The composition and properties of the borated paraffin, Pu-Be source, plastic container and 3-He detector were either supplied by the manufacturer or taken from compendium material composition data [13]. The atomic composition of the samples was determined from the oxide composition of the starting materials given in Table 2.1, as proposed by Piotrowski *et al* [2]. The atomic compositions of the different materials used in MCNP modeling of the experimental setup are provided in Table 2.3.

2.3.2. Neutron Source. To simulate the Pu-Be source used in the experiment an isotropic volumetric source was implemented. Unfortunately, the initial plutonium

isotopic abundances of the Missouri S&T's neutron source are unknown; therefore, the current neutron flux and the energy distribution of the source remain uncertain. Since measuring the neutron energy spectrum of the source was beyond the scope of this work, a spectrum adapted from the work of Harvey *et al* [13] was used in the present study for simulation purposes. The neutron spectrum was approximated by a histogram with an energy resolution of 0.5 MeV as shown in Figure 2.3.

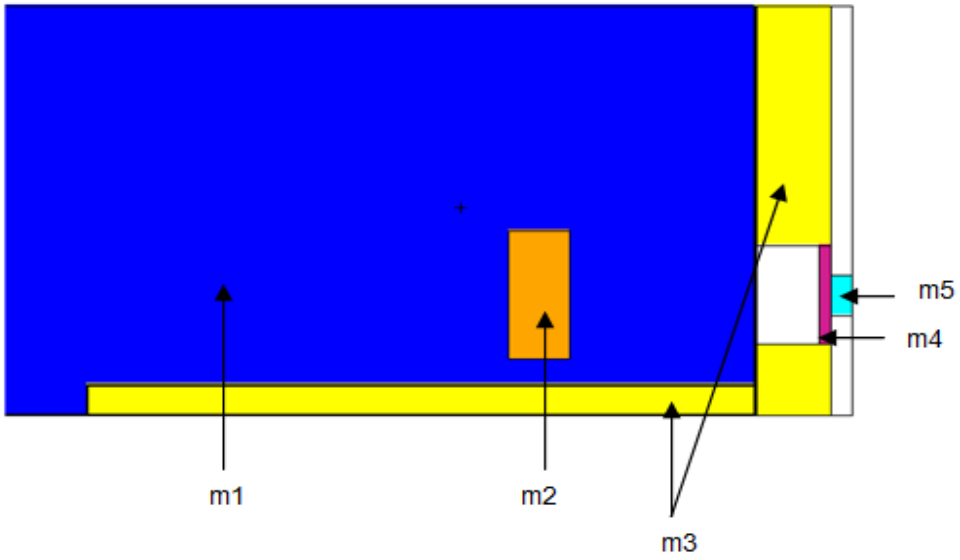

Figure 2.2 Geometry of the experimental arrangement in MCNP; m1-water, m2-Pu-Be source, m3- borated paraffin, m4-cement sample, and m5-H3 detector

2.3.3. Determination of the Reaction Rate. The estimate of the neutron flux in the cell describing the detector was scored with a track length F4 tally. The tally multiplier FM card was also used to estimate the absorption reaction rate in the detector cell which corresponds to the actual nuclear reaction by which thermal neutrons are detected in Helium 3-proportional counters, this is:

$$^{3}He + {}^{1}n \rightarrow {}^{3}H\ (0.191\ MeV) + {}^{1}p\ (0.573\ MeV) \qquad (2)$$

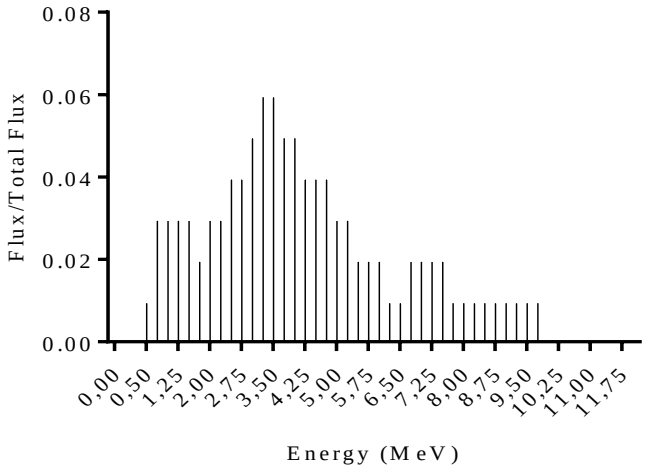

Figure 2.3 Neutron energy spectrum of the Pu-Be source [13]

Table 2.3 Atomic composition and density of the materials used in the simulation

Material	Atomic Composition (%)	Density (g/cm^3)
Water	H (11.90%), O (88.1%)	1
PuBe Source	Pu-239 (66.93%), Be (33.07%)	2.9
Plexiglass	H (8%), C (59.98%) O (31.96%)	1.19
Detector	He-3 (80%), Kr-78(0.07%), Kr-80 (0.45%), Kr-82 (2.32%), Kr-83(2.3%), Kr-84(11.4%), Kr-86 (3.46%)	0.008056
Borated Paraffin	C (31.6%), H (31.6%), Na (7.6%), B-10 (3.2%), B-11 (12.3%), O (13.7%)	0.93
Sample 1	H (3.17%), Si (6.81%), O (50.90%), Al (1.64%), Fe (1.53%), Ca (33.80%), Mg (1.27%), S (0.87%)	1.8
Sample 2	H (3.15%), Si (6.77%), O (50.63%), Al (1.63%), Fe (1.52%), Ca (33.55%), Mg (1.26%), S (0.87%), Sm-144 (0.02%), Sm-147 (0.09%), Sm-148 (0.07%), Sm-149 (0.09%), Sm-150 (0.05%), Sm-152 (0.17%), Sm-154 (0.14%)	2
Sample 3	H (3.06%), Si (6.57%), O (49.55%), Al (1.58%), Fe (1.48%), Ca (32.57%), Mg (1.22%), S (0.84%), Sm-144 (0.10%), Sm-147 (0.47%), Sm-148 (0.35%), Sm-149 (0.43%), Sm-150 (0.23%), Sm-152 (0.83%), Sm-154 (0.71%)	2.33
Sample 4	H (2.94%), Si (6.31%), O (48.17%), Al (1.52%), Fe (1.42%), Ca (31.31%), Mg (1.17%), S (0.81%), Sm-144 (0.19%), Sm-147 (0.95%), Sm-148 (0.71%), Sm-149 (0.88%), Sm-150 (0.47%), Sm-152 (1.70%), Sm-154 (1.44%)	2.29
Sample 5	H (2.69%), Si (5.78%), O (45.27%), Al (1.39%), Fe (1.30%), Ca (28.68%), Mg (1.08%), S (0.74%), Sm-144 (0.4%), Sm-147 (1.96%), Sm-148 (1.47%), Sm-149 (1.81%), Sm-150 (0.96%,) Sm-152 (3.50%), Sm-154 (2.97%)	2.1

3. RESULTS AND DISCUSSION

3.1. DENSITY MEASUREMENTS

Figure 3.1 gives the density for the five composites analyzed in this study. Initially the addition of samarium oxide increases the density of the samples until it reaches a maximum value when 10 wt% of the oxide is added to the cement paste. Beyond this point, the density decreases.

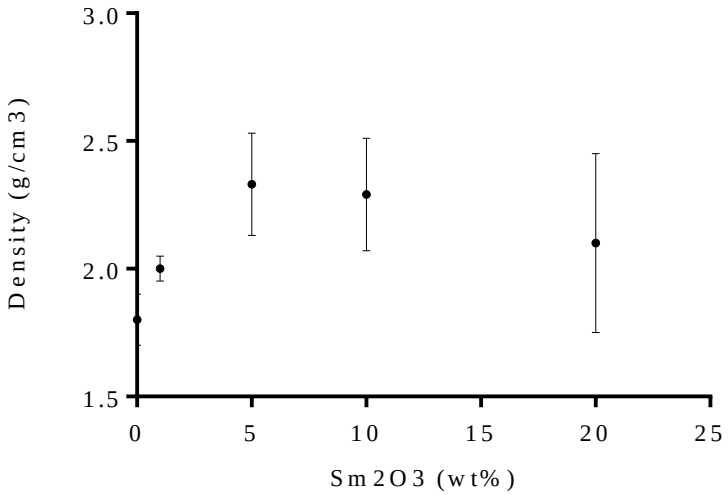

Figure 3.1 Density Sm2O3-WOPC composites

3.2. TRANSMISSION EXPERIMENTS

Table 3.1 gives the effective cross sections for the composites calculated from the experimental measurements. The results show that the addition of Sm_2O_3 enhances the attenuation properties of white ordinary Portland cement. Linear regression analysis of the experimental data is shown in Figure 3.2 The correlation between the content of Sm_2O_3 and the effective cross section of each sample is given by the following equation:

$$\sum_{eff} = 0.178 \times (\mathrm{Sm_2O_3}\ wt\%) + 0.893 \quad (3)$$

where $\sum_{eff}$ is the effective neutron cross section and $Sm_2O_3\ wt\%$ is the weight fraction of samarium oxide used for the fabrication of the composite.

Table 3.1 Results neutron attenuation properties of WOPC- Sm2O3 composites

Sample	wt% Sm2O3	Io (counts)	I (counts)	Thickness (cm)	Effective Cross Section (cm^{-1})
S1	0	40616	29721	0,606552	0,5149
S2	1	40616	26660	0,63119	0,6669
S3	5	40616	8919	0,63246	2,3969
S4	10	40616	5236	0,62534	3,2759
S5	20	40616	4257	0,56134	4,0182

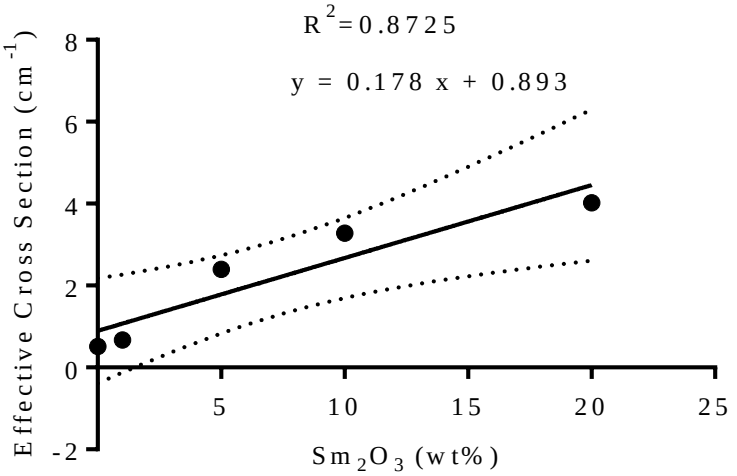

Figure 3.2 Variation of the neutron effective cross section with Sm2O3 content

3.3. MCNP SIMULATIONS

Figure 3.3 shows the PuBe neutron spectrum at the sample location (20 cm from the source) when the source is moderated by water. Due to the interaction between the source neutrons with water, the amount of high energy neutrons is reduced and epithermal and thermal neutrons show up in the spectrum being larger than those noticed with the bare source. This result demonstrates that the moderation process used in this

study was efficient for slowing down the fast neutrons to thermal and epithermal energies.

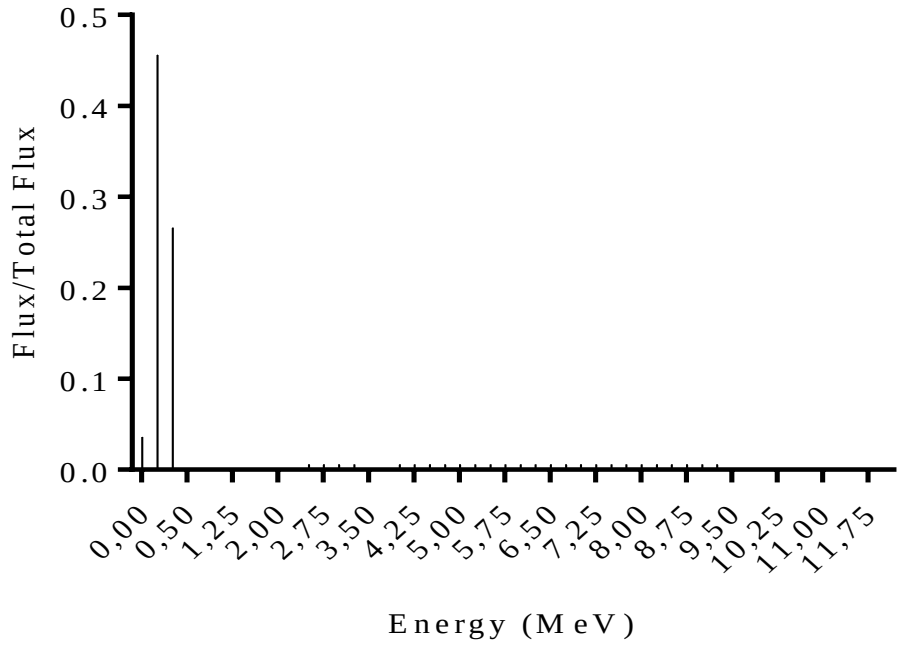

Figure 3.3 PuBE neutron spectrum at the source location when the source is submerged in water

Table 3.2 shows the comparison between the effective thermal cross sections of the composites obtained by experimental data and MCNP simulations. The simulations confirm that the cement composites with samarium oxides have better attenuation properties for thermal neutrons. In general, there exists good agreement between the results obtained by the experiments and the MCNP simulations. Yet, the results obtained from simulations tend to be lower than those measured. The reason for these differences is probably due to the simplifications and assumptions made in the simulation geometry. Likewise, the difference in the chemical composition between the actual composite slab and those utilized in the Monte Carlo simulation could contribute to the difference between the measured and simulation results.

Table 3.2 Comparison between experimental and simulation results

Sample	Sm2O3 wt%	Exp XS (cm^{-1})	MCNP XS (cm^{-1})	RD (%)
S1	0	0.51489	0.47888	7.4
S2	1	0.66699	0.68195	2.2
S3	5	2.39695	2.20195	8.5
S4	10	3.27598	2.98527	9.3
S5	20	4.01823	3.73894	7.2

4. CONCLUSIONS

The neutron attenuation properties of white ordinary Portland cement modified with samarium oxide were studied. The results reveal that samarium oxide is an effective additive to enhance the neutron attenuation properties of cement against thermal neutrons. This is attributable to the high absorption cross section of the isotope Sm-149 present in naturally occurring samarium oxide. The results also show that increasing the concentration of samarium oxide makes the cement paste more effective for shielding of thermal neutrons. A linear correlation was observed between the effectiveness of the shielding and the concentration of samarium oxide in the paste.

The addition of samarium oxide also affects the density of the cement composites. However, the density seems to play little effect on the neutron attenuation capability of the samples because the highest effective thermal cross section was obtained for sample with the highest samarium concentration (WOPC+ Sm_2O_3 50 wt%) and not for the paste with the highest density (WOPC+ Sm_2O_3 10 wt%). This result demonstrates that optimizing the chemical composition with high absorbing elements is more effective than increasing density of the of the cement pastes for attenuation of thermal neutrons.

From the calculation and the validation of the experiment performed it is clear that the Monte Carlo method is a feasible numerical technique to predict the attenuation properties of Sm_2O_3-WOPC composites. Both experimental and simulation results show good agreement with small differences which are probably attributable to the difference between the modeled and the actual PuBe neutron source as well as the difference between the simulated and real composition of the cement pastes.

Although cement pastes modified with samarium oxide show better attenuation properties with respect to thermal neutrons, it is necessary to evaluate other structural properties that are also important for shielding applications. Likewise, it is recommended to study the gamma ray shielding capability of the WOPC- Sm_2O_3 and to use additional additives that can improve the attenuation properties of the cement paste even further.

REFERENCES

[1] S. M. Malkapur, H. Satdive, M. C. Narasimhan, N. B. Karkera, P. Goverdhan, and V. Sathian, "Effect of mix parameters and hydrogen loading on neutron radiation shielding characteristics of latex modified concrete mixes," *Prog. Nucl. Energy*, vol. 83, pp. 8–12, 2015.

[2] T. Piotrowski, M. Mazgaj, A. Żak, and J. Skubalski, "Importance of Atomic Composition and Moisture Content of Cement based Composites in Neutron Radiation Shielding," *Procedia Engineering*, vol. 108. pp. 616–623, 2015.

[3] E. Gallego, A. Lorente, and H. R. Vega-Carrillo, "Testing of a high-density concrete as neutron shielding material," *Nucl. Technol.*, vol. 168, no. 2, pp. 399–404, 2009.

[4] J. Wang, G. Li, and D. Meng, "Evaluation of the performance of peridotite aggregates for radiation shielding concrete," *Ann. Nucl. Energy*, vol. 71, pp. 436–439, 2014.

[5] E. Calzada, F. Grünauer, B. Schillinger, and H. Türck, "Reusable shielding material for neutron- and gamma-radiation," *Nucl. Instruments Methods Phys. Res. Sect. A Accel. Spectrometers, Detect. Assoc. Equip.*, vol. 651, no. 1, pp. 77–80, 2011.

[6] R. Küçer and N. Küçer, "Neutron Shielding Properties of Concretes Containing Boron Carbide and Ferro – Boron," vol. 195, pp. 1752–1756, 2015.

[7] T. Piotrowski, D. B. Tefelski, J. Skubalski, and A. Żak, "Experiments on Neutron Transport through Concrete Member and the Potential for the Use in Material Investigation," *Acta Phys. Pol. A*, vol. 128, no. 2B, p. B–14–B–19, 2015.

[8] H. A. Colorado, J. Pleitt, J.-M. Yang, and C. H. Castano, "Boron and Lead Based Chemically Bonded Phosphates Ceramics for Nuclear Waste and Radiation Shielding Applications," *Adv. Mater. Sci. Environ. Energy Technol. II*, no. August 2013, pp. 1–9, 2013.

[9] P. Wang, X. Tang, H. Chai, D. Chen, and Y. Qiu, "Design , fabrication , and properties of a continuous carbon-fiber reinforced Sm 2 O 3 / polyimide gamma ray / neutron shielding material," vol. 101, pp. 218–225, 2015.

[10] B. S. Seshadri, V. Venkatesam, and V. Sundararaman, "Spectra of D-T neutrons transmitted through rare earth mixed concretes," *Nucl. Eng. Des.*, vol. 97, no. 2, pp. 223–232, Nov. 1986.

[11] T. Piotrowski, D. B. Tefelski, J. J. Sokołowska, and B. Jaworska, "NGS-concrete - new generation shielding concrete against ionizing radiation - the potential evaluation and preliminary investigation," *Acta Phys. Pol. A*, vol. 128, no. 2, pp. 9–13, 2015.

[12] “MCNP—A General Monte Carlo N-Particle Transport Code-Version 6.1.” Los Alamos National Laboratory, 2013.

[13] Harvey, Zachary R., "Neutron flux and energy characterization of a plutonium-beryllium isotopic neutron source by Monte Carlo simulation with verification by neutron activation analysis" (2010).

SECTION

4. CONCLUSIONS AND FUTURE WORK

4.1. CONCLUSIONS

The structural, mechanical and attenuation properties of cement pastes modified with magnetite powder were studied to reveal the effect of fine aggregates on the mechanical and shielding characteristics of cementitious matrices. Composites were prepared via wet chemistry using different proportions of magnetite powder. The microstructure of the samples was characterized using scanning electron microscopy (SEM) and x-ray diffraction (XRD). The XRD results show that magnetite particles did not interact chemically with the cement matrix to form new radical phases. Also, magnetite contents increase in samples with the magnetite loading. The SEM micrographs show that at magnetite loadings of 20 wt%, there is good dispersion of the particles through the cement matrix; however, further increase in the magnetite loading leads to agglomeration of the particles making the cement matrix more heterogeneous.

It was also found that addition of magnetite to white ordinary Portland cement pastes affects the stress-strain response of the samples. Composites with 1% and 20% by weight of magnetite exhibited the same kind of brittle behavior obtained for the plain WOPC paste; although, these pastes showed a higher peak stress with respect to the control sample. A more ductile behavior was observed in composites prepared with magnetite additions of 2.5%, 5%, 10%, and 40%. For all these samples, the peak stress and the strain corresponding to peak stress were enhanced with respect to the plain WOPC control sample. Further improvements in toughness are also achieved for the samples with ductile behavior.

Gamma ray attenuation measurements demonstrated that the addition of magnetite has little effect on the attenuation properties of the composite at 0.662 MeV. At this energy, the predominant attenuation mechanism in the samples is Compton scattering; therefore, the compositional effect upon the attenuation characteristics of the samples is small and the differences in the attenuation properties among the fabricated samples are small too.

The neutron attenuation properties of white ordinary Portland cement modified with samarium oxide were also studied. The results reveal that samarium oxide is an effective additive to enhance the neutron attenuation properties of cement against thermal neutrons. This is attributable to the high absorption cross section of the isotope Sm-149 present in naturally occurring samarium oxide. The results also show that increasing the concentration of samarium oxide makes the cement paste more effective for shielding of thermal neutrons. A linear correlation was observed between the effectiveness of the shielding and the concentration of samarium oxide in the paste.

The addition of samarium oxide also affects the density of the cement composites. However, the density seems to play little effect on the neutron attenuation capability of the samples because the highest effective thermal cross section was obtained for sample with the highest samarium concentration (WOPC+ Sm_2O_3 50 wt%) and not for the paste with the highest density (WOPC+ Sm_2O_3 10 wt%). This result demonstrates that optimizing the chemical composition with high absorbing elements is more effective than increasing density of the of the cement pastes for attenuation of thermal neutrons.

Although cement pastes modified with samarium oxide show better attenuation properties with respect to thermal neutrons, it is necessary to evaluate other structural properties that are also important for shielding applications. Likewise, it is recommended to study the gamma ray shielding capability of the WOPC- Sm_2O_3 and to use additional additives that can improve the attenuation properties of the cement paste even further.

4.2. FUTURE WORK

The following are some of the areas that required further work:

- More gamma ray transmission experiments must be conducted using sample of different thickness and gamma ray sources with multiple photopeaks such as Co-60 (1.173 and 1.333 MeV) or multisotopic Europium source (Eu-152, Eu-154 and Eu-155) which present 14 different peaks. By doing this, it will be possible not only to better characterize the attenuation properties at a given energy, but also to study the shielding capabilities of the samples over energy ranges where other attenuation mechanisms such as photoelectric effect or pair production become more important. In those cases, the difference in the chemical composition of the samples is expected to affect the attenuation properties of the composites to a greater extend.

- If a multipeak gamma source is used for the transmission experiment, it is advisable to use a high purity germanium detector (HPGe) instead of the NaI detector used in this work. The higher resolution of the HPGe will allow unfolding the gamma spectra more efficiently. Also, it is recommended to use commercial gamma spectroscopy software to fit the peaks and obtain and accurate estimation of their net area. The procedure for net peak area evaluation used in this work is appropriate for simple spectrum like the one obtained for the Cs-137 source; however, it fails when multiple peaks pile up together.
- The MCNP code can be used to optimize parameters of the geometry for the gamma transmission experiment such as the distance between the collimators, the distance between the source and the detector and so on. By doing this, it will be easier to obtain a better approximation of the narrow beam geometry that is required for transmission experiments. The MCNP also needs to be enhanced to include more accurate details of the experimental setup. A better representation of the NaI detector will provide more accurate values for the energy deposited in the real experiments and therefore better estimates of the attenuation properties of the samples will be obtained.
- The experimental setup used in this work for neutron measurements only gives a rough estimate of the attenuation properties of the composites against thermal and epithermal neutrons. For better characterization of the attenuation properties, it is recommended to use other systems such as a neutron generator or a neutron diffractometer to create a monochromatic beam of neutrons for the transmission experiment. This will help to obtain the actual thermal and fast neutron removal cross section of the samples instead of the effective cross section.
- The current MCNP model must be updated to include the actual chemical composition and energy neutron spectrum of the PuBe source. To do so, the energy neutron spectrum of the source must be measured experimentally by neutron activation analysis of different foils. Additionally, the simulation model can be also used to optimize some geometry parameters of the transmission experiment such as the distance between the paraffin collimator and the source, the position of the Helium-3 detector, among others.

APPENDIX A.
PEAK AREA DETERMINATION

The net area of the gamma ray peak for the Cs-137 spectrum was determined by simply adding up the counts from each of the channel in the peak range and then subtracting the contribution of the continuum background in which the peak lies. The contribution of the continuum background was determined by averaging on two clean regions of the spectrum as shown in figure A.1. In this approach, the uncertainty in the peak area assumed to be simply due to statistical fluctuations in the areas determined. If the area of the peak is A, the full width of the peak (in channels) is W_p, the area of the background only region is B and its width W_B, then the net peak area (N) is:

$$N = A - B\frac{W_p}{W_b} \tag{A.1}$$

And, keeping in mind that $\sigma_A^2 = A$ and $\sigma_B^2 = B$, the uncertainty is given by:

$$\sigma_N = \sqrt{A + B\left(\frac{W_P}{W_B}\right)^2} \tag{A.2}$$

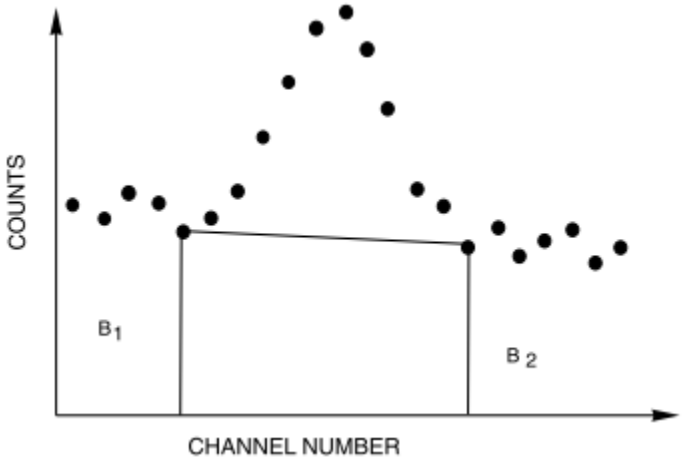

Figure A.1. Net Area Determination

APPENDIX B.
PROPAGATION OF UNCERTAINTY

The uncertainty of the mass attenuation coefficient was determined using the error propagation rules. First, error propagation was applied to the Lambert-Beers law which is given by:

$$\mu = \left(-\frac{1}{x}\right) \ln\left(\frac{I}{I_0}\right) \tag{B.1}$$

Where x is the thickness of the attenuator, and I_0 and I are the incident and attenuated beam intensities respectively. Assuming that the variables are independent, the standard deviation of the linear attenuation coefficient can be expressed as follows:

$$\sigma_\mu^2 = \left(\frac{\delta\mu}{\delta x}\right)\sigma_x^2 + \left(\frac{\delta\mu}{\delta I}\right)\sigma_I^2 + \left(\frac{\delta\mu}{\delta I_0}\right)\sigma_{I_0}^2 \tag{B.2}$$

An analogous procedure was then used to calculate the standard deviation of the mass attenuation coefficient (MAC). Error propagation was applied to the MAC equation which is given by:

$$MAC = \frac{\mu}{\rho} \tag{B.3}$$

Assuming independent variables the standard deviation of the MCA is obtained by:

$$\sigma_{MAC}^2 = \left(\frac{\delta MAC}{\delta\mu}\right)\sigma_\mu^2 + \left(\frac{\delta MAC}{\delta\rho}\right)\sigma_\rho^2 \tag{B.4}$$

APPENDIX C.
MCNP INPUT DECKS

The following two MCNP input decks were used for the gamma rays and neutron calculations:

```
1mcnp     version 6     ld=05/08/13                  05/05/16 09:49:42

************************************************************************
*              probid =  05/05/16 09:49:42

 i=sample.txt tasks 8

      1-      Linear Afftenuatuion Coefficient
      2-      c
      3-      c ------------------CELL CARD-------------------------
      4-      1   0  -1 5 -8 imp:p=1   $ Beam 1
      5-      2   0  -1 -4 2 imp:p=1   $ Beam 2
      6-      3   0 1 2 -3 -9 10 -12 11 imp:p=1   $ Before Collimator
      7-      4   1 -11.34 1 3 -4 -9 10 -12 11 VOL=496.07 imp:p=1   $ Collimator 1
      8-      5   2 -1.7 -20 4 -5 imp:p=4 $ sample
      9-      6   0  4 -6 -9 10 -12 11 1 (20:5) imp:p=1 $Between collimators
     10-      7   1 -11.34 1 6 -7 -9 10 -12 11 VOL=496.07 imp:p=1 $ Collimator 2
     11-      8   0  1 7 -8 -9 10 -12 11 imp:p=1 $ After Collimator 2
     12-      c 9   0   7 -8 -1 imp:p=4 $ Detector
     13-      10 0 -2:8:-11:12:9:-10 imp:p=0 $ Outside Kill all photons
     14-      c
     15-
     16-      c ------------------SURFACE CARDs-------------------------
     17-      1   cy 0.5        $ Diameter hole
     18-      2   py 0         $ Left border
     19-      3   py 1
     20-      4   py 6
     21-      5   py 6.6424
     22-      6   py 11
     23-      7   py 16
     24-      8   py 17
     25-      9   px 10
     26-      10  px -10
     27-      11  pz -2.5
     28-      12  pz 2.5
     29-      13 cy 2.5
     30-      14 py 15.5
     31-      20 cy 2.5
     32-      c
     33-      c ------------------DATA CARD-------------------------
     34-      c
     35-      mode p                        $ photon mode only
```

```
36-     nps 100000000                   $ number of histories  to be run
37-     c
38-     c -----------Europium Gamma Ray Source------------------
39-     SDEF POS 0 0.5 0  PAR=2 ERG= 0.662                              $ pos
40-     c ------------------DETECTORS--------------------------
41-     f2:p  7                 $ Average surface flux
42-     sd2  100
43-     ft2   INC
44-     fu2   0  10000  T             $ tally: uncollided & collided dose
45-     c
46-     c ------------------MATERIALS--------------------------
47-     c ---------Pb sample (density 11.34 g/cm^3)-----------
48-     m1 82206 0.24100 82207 0.22100 82208 0.52400   $Lead
49-     m2  14000   -0.064                      $  %wt Si
50-          8016  -0.4925                       $  %wt O
51-          13000 -0.0156                        $  %wt Al
52-          26000 -0.0630                       $  %wt Fe
53-          20000 -0.3150                       $  %wt Ca
54-          12000 -0.0120                       $  %wt Mg
55-          16000 -0.0081                       $  %wt S
56-          1001  -0.0294                      $  %wt H
57-          25000 -0.0005
58-     c
```

1- Neutron Experiments

```
2-      c
3-      c ------------------CELL CARD--------------------------
4-      c mat  rho (g/cc) surfaces            importance
5-      c mat  rho (g/cc) surfaces            importance
6-      1 4   -1.19  10 -11 -15 17 20 -18    imp:n=1 $Tank
7-      2 4   -1.19  -12 13 -15 17 20 -18    imp:n=1 $Tank
8-      3 4   -1.19  20 -19 -14 16 -10 12    imp:n=1 $Tank
9-      4 4   -1.19  -16 17 -10 12 20 -18    imp:n=1 $Tank
10-     5 4   -1.19  14 -15 -10 12 20 -18    imp:n=1 $Tank
11-     6 2   -1     -10 12 -14 16 19 -21 #11 #8   imp:n=8 $Water
12-     7 3   -0.93   11 -30 -14 16 20 -32 31  imp:n=8 $Paraffin
13-     8 3   -0.93   19 -40 -10 43 -41 42    imp:n=8 $  $Paraffin
14-     9 1   -2.29  44 -30 -31 imp:n=10 $sample
15-     10 5  -0.008056515 30 -46 -45 imp:n=12 $detector
16-     11 6  -2.90 49 -48 -47 imp:n=8 $PuBe source
17-     12 0 (13 -46 -18 20 -15 17) #1 #2
18-          #3 #4 #5 #6 #7 #8 #9 #10 #11 imp:n=8  $air
19-     13 0 (-13:46:18:-20:15:-17) imp:n=0
20-
21-     c ----------------- SURFACE CARDS---------------------
```

```
C Plaxiglass Tank
10 py 17
11 py 17.05
12 py -44
13 py -44.05
14 px 17.05
15 px 18
16 px -17.05
17 px -18
18 pz 36
19 pz -6
20 pz -6.05
21 pz 17
c Paraffin Wax
30 py 20.55
31 cy 2.5
32 pz 14.5
40 pz -4.5
41 px 10.5
42 px -10.5
43 py -21
44 py 19.924652
45 cy 1
46 py 21.55
c source
47 cz 1.64
48 pz 4.09
49 pz -4.09
c outside of everything
100 so 100

c ------------------DATA CARD--------------------------
c
mode n                      $ neutron mode only
nps 1e8                     $ number of histories  to be run
c
c Source Definition
SDEF POS=0 0 -4.09 AXS= 0 0 1 ERG=d1 RAD=d2 EXT=d3
si1 h 0 .25
     .5
     .75
     1
     1.25
     1.5
     1.75
     2
```

68- 2.25
69- 2.5
70- 2.75
71- 3
72- 3.25
73- 3.5
74- 3.75
75- 4
76- 4.25
77- 4.5
78- 4.75
79- 5
80- 5.25
81- 5.5
82- 5.75
83- 6
84- 6.25
85- 6.5
86- 6.75
87- 7
88- 7.25
89- 7.5
90- 7.75
91- 8
92- 8.25
93- 8.5
94- 8.75
95- 9
96- 9.25
97- 9.5
98- 9.75
99- 10
100- 10.25
101- 10.5
102- 10.75
103- 11
104- 11.25
105- 11.5
106- 11.75
107- 12
108- SP1 d 0 2.39E-4
109- 4.95E-3
110- 1.29E-2
111- 1.69E-2
112- 1.73E-2
113- 1.54E-2

```
114-        1.17E-2
115-        1.59E-2
116-        1.93E-2
117-        2.15E-2
118-        2.62E-2
119-        3.84E-2
120-        4.96E-2
121-        5.22E-2
122-        5.01E-2
123-        4.72E-2
124-        4.49E-2
125-        4.32E-2
126-        4.13E-2
127-        3.89E-2
128-        3.35E-2
129-        2.76E-2
130-        2.49E-2
131-        2.40E-2
132-        2.09E-2
133-        2.12E-2
134-        2.39E-2
135-        2.50E-2
136-        2.50E-2
137-        2.49E-2
138-        2.43E-2
139-        2.30E-2
140-        2.11E-2
141-        1.94E-2
142-        1.82E-2
143-        1.75E-2
144-        1.67E-2
145-        1.47E-2
146-        1.13E-2
147-        7.08E-3
148-        3.98E-3
149-        2.57E-3
150-        1.34E-3
151-        4.27E-4
152-        5.93E-6
153-        1.23E-8
154-        9.78E-9
155-        7.74E-9
156-    si2 0 1.64
157-    sp2 -21 1
158-    si3 0 8.18
159-    sp3 -21 0
```

```
c Detector
F4:n 10
FM4 (3.14159E+00) (-3.14159E+00 5 (-2))
c FT4   INC
c FU4   0 1000 T
E4 2.5e-8 4.140e-7 .25 .5 .75 1 1.25 1.5
     1.75 2 2.25 2.5 2.75 3 3.25
     3.5 3.75 4 4.25 4.5 4.75 5
     5.25 5.5 5.75 6 6.25 6.5 6.75
     7 7.25 7.5 7.75 8 8.25 8.5
     8.75 9 9.25 9.5 9.75 10 10.25
     10.5 10.75 11 11.25 11.5 11.75
     12
c
c ----------------- METERIALS----------------------
c sample
m1   1001.70c  -0.0294    $  Hydrogen                    $  Hydrogen
     14000.42c -0.0631  $ Silicon
     8016.70c  -0.4817 $ Oxygen
     13027.70c -0.0152  $ Aluminum
     26000.42c -0.0142  $ Iron
     20000.24c -0.3131 $ Calcium
     12000.42c -0.0117 $ Magnesium
     16000.60c -0.0081  $ Sulfur
     62144.70c -0.0019 $ Sm 144
     62147.70c -0.0095  $ Sm 147
     62148.70c -0.0071  $ Sm 148
     62149.70c -0.0088  $ Sm 149
     62150.70c -0.0047  $ Sm 150
     62152.70c -0.017 $ Sm 152
     62154.70c -0.00144  $ Sm 154
c water
m2 1001.70c -0.1190 $ Hydrogen
    8016.70c -0.88810 $Oxygen
c Boraffin rho=0.93 g/cc
m3 6000.70c 0.316
     1001.70c 0.316
     11023.70c 0.076923077
     5010.70c  0.030615385
     5011.70c  0.123230769
     8016.70c  0.137307692
c Plexiglass
m4 1001.70c 0.080538
    6000.70c 0.599848
    8016.70c 0.319614
c Detector
```

```
206-      m5 2003.70c -0.8
207-           36078.70c -0.0007
208-           36080.70c -0.0045
209-           36082.70c -0.0232
210-           36083.70c -0.023
211-           36084.70c -0.114
212-           36086.70c -0.0346
213-      C Pu-Be Source rho=2.9 g/cc
214-      m6 94239.66c -0.6693
215-          4009.66c -0.3307
```

REFERENCES

[1] J. E. Turner, *Atoms, Radiation, and Radiation Protection*. Weinheim, Germany: Wiley-VCH Verlag GmbH & Co. KGaA, 2007.

[2] S. N. Ahmed, "Interaction of radiation with matter," in *Physics and Engineering of Radiation Detection*, Elsevier, 2015, pp. 65–155.

[3] S. Nambiar and J. T. W. Yeow, "Polymer-composite materials for radiation protection," *ACS Appl. Mater. Interfaces*, vol. 4, no. 11, pp. 5717–5726, 2012.

[4] R. D. Evans, *The Atomic Nucleus*. New York: McGraw-Hill, 1955.

[5] S. N. Ahmed, *Physics and Engineering of Radiation Detection*, 2nd Editio. Elsevier, 2014.

[6] L. Anderson, "Compton Scattering." pp. 1–13, 2007.

[7] http://ocw.mit.edu/courses/nuclear-engineering/22-01-introduction-to-ionizing-radiation-fall-2006/lecture-notes/energy_dep_photo.pdf.

[8] P. Wang, X. Tang, H. Chai, D. Chen, and Y. Qiu, "Design , fabrication , and properties of a continuous carbon-fiber reinforced Sm 2 O 3 / polyimide gamma ray / neutron shielding material," vol. 101, pp. 218–225, 2015.

[9] S. Alhajali, S. Yousef, and B. Naoum, "Appropriate concrete for nuclear reactor shielding," *Appl. Radiat. Isot.*, vol. 107, no. 4, pp. 29–32, Jan. 2016.

[10] S. Sato, T. Maegawa, K. Yoshimatsu, K. Sato, A. Nonaka, K. Takakura, K. Ochiai, and C. Konno, "Development of a low activation concrete shielding wall by multi-layered structure for a fusion reactor," *J. Nucl. Mater.*, vol. 417, no. 1–3, pp. 1131–1134, 2011.

[11] "http://matse1.matse.illinois.edu/concrete/glos.html." .

[12] S. A. Abo-El-Enein, H. A. El-Sayed, A. H. Ali, Y. T. Mohammed, H. M. Khater, and A. S. Ouda, "Physico-mechanical properties of high performance concrete using different aggregates in presence of silica fume," *HBRC J.*, vol. 10, no. 1, pp. 43–48, 2014.

[13] O. Gencel, A. Bozkurt, E. Kam, and T. Korkut, "Determination and calculation of gamma and neutron shielding characteristics of concretes containing different hematite proportions," *Ann. Nucl. Energy*, vol. 38, no. 12, pp. 2719–2723, 2011.

[14] I. Akkurt, C. Basyigit, S. Kilincarslan, and B. Mavi, "The shielding of ??-rays by concretes produced with barite," *Prog. Nucl. Energy*, vol. 46, no. 1, pp. 1–11, 2005.

[15] B. Oto, N. Yildiz, T. Korkut, and E. Kavaz, “Neutron shielding qualities and gamma ray buildup factors of concretes containing limonite ore,” *Nucl. Eng. Des.*, vol. 293, pp. 166–175, 2015.

[16] A. M. El-Khayatt, “Radiation shielding of concretes containing different lime/silica ratios,” *Ann. Nucl. Energy*, vol. 37, no. 7, pp. 991–995, 2010.

[17] E. Horszczaruk, P. Sikora, and P. Zaporowski, “Mechanical properties of shielding concrete with magnetite aggregate subjected to high temperature,” *Procedia Eng.*, vol. 108, pp. 39–46, 2015.

[18] S. M. R. Aghamiri, S. M. J. Mortazavi, M. A. M. Shirazi, F. Rahmani, A. Amiri, and S. Jarideh, “Production of a novel high strength heavy concrete using tourmaline and galena for neutron and photon radiation shielding,” *Int. J. Radiat. Res.*, vol. 12, no. 3, pp. 277–282, 2014.

[19] D. Rezaei-Ochbelagh and S. Azimkhani, “Investigation of gamma-ray shielding properties of concrete containing different percentages of lead,” *Appl. Radiat. Isot.*, vol. 70, no. 10, pp. 2282–2286, 2012.

[20] S. Ristinah and L. Djakfar, “Evaluation of the Characteristic of Heavyweight Concrete using Steel Slag Aggregates for Radiation Shielding,” vol. 1, no. 11, pp. 512–521, 2011.

[21] D. Sarıyer, R. Küçer, and N. Küçer, “Neutron Shielding Properties of Concretes Containing Boron Carbide and Ferro – Boron,” *Procedia - Soc. Behav. Sci.*, vol. 195, pp. 1752–1756, 2015.

[22] M. H. Kharita, S. Yousef, and M. Alnassar, “Review on the addition of boron compounds to radiation shielding concrete,” *Prog. Nucl. Energy*, vol. 53, no. 2, pp. 207–211, 2011.

[23] B. S. SESHADRI, “Transmission Measurements of D-T Neutrons through Gadolinium Loaded Concrete and Polypropylene,” *J. Nucl. Sci. Technol.*, vol. 26, no. 9, pp. 881–886, 1989.

[24] T. Piotrowski, D. B. Tefelski, J. J. Sokołowska, and B. Jaworska, “NGS-concrete - new generation shielding concrete against ionizing radiation - the potential evaluation and preliminary investigation,” *Acta Phys. Pol. A*, vol. 128, no. 2, pp. 9–13, 2015.

[25] B. S. Seshadri, V. Venkatesam, and V. Sundararaman, “Spectra of D-T neutrons transmitted through rare earth mixed concretes,” *Nucl. Eng. Des.*, vol. 97, no. 2, pp. 223–232, Nov. 1986.

[26] B. S. Seshadri and R. Venkatesan, “Transmission characteristics of Cf252 neutrons passing through rare earth and boron loaded concrete slab shields,” *Nucl. Eng. Des.*, vol. 117, no. 3, pp. 325–331, Dec. 1989.

[27] T. Piotrowski, D. B. Tefelski, M. Mazgaj, J. Skubalski, A. Żak, and J. J. Sokołowska, “Polymers in Concrete – The Shielding against Neutron Radiation,” *Adv. Mater. Res.*, vol. 1129, pp. 131–138, Nov. 2015.

[28] S. Chuah, Z. Pan, J. G. Sanjayan, C. M. Wang, and W. H. Duan, “Nano reinforced cement and concrete composites and new perspective from graphene oxide,” *Constr. Build. Mater.*, vol. 73, pp. 113–124, 2014.

[29] I. Journal, M. Science, and E. Vol, “Novel Method for Radiation Shielding Using Nano-Concrete Composite,” vol. 1, no. 1, pp. 23–26, 2013.

[30] H. E. Hassan, H. M. Badran, A. Aydarous, and T. Sharshar, “Studying the effect of nano lead compounds additives on the concrete shielding properties for ??-rays,” *Nucl. Instruments Methods Phys. Res. Sect. B Beam Interact. with Mater. Atoms*, vol. 360, pp. 81–89, 2015.

[31] V. V. Belyakov, V. A. Grigor’ev, P. A. Lavdanskii, O. A. Remeiko, and V. F. Khokhlov, “Calculation of shielding made of concrete with an increased hydrogen content,” *Sov. At. Energy*, vol. 44, no. 5, pp. 526–528, May 1978.

[32] G. Gündüz, “Colemanite-baryte frit and polymer impregnated concrete as shielding materials,” *Nucl. Eng. Des.*, vol. 72, no. 3, pp. 439–447, Oct. 1982.

[33] S. M. A. Islam, M. M. Akramuzzaman, M. A. Awal, and M. N. Islam, “A study of neutron shielding properties of some multilayers containing polyethylene,” *Appl. Radiat. Isot.*, vol. 44, no. 8, pp. 1161–1164, Aug. 1993.

[34] M. H. Kharita, S. Yousef, and M. AlNassar, “The effect of the initial water to cement ratio on shielding properties of ordinary concrete,” *Prog. Nucl. Energy*, vol. 52, no. 5, pp. 491–493, Jul. 2010.

[35] R. Şahin, R. Polat, O. İçelli, and C. Çelik, “Determination of transmission factors of concretes with different water/cement ratio, curing condition, and dosage of cement and air entraining agent,” *Ann. Nucl. Energy*, vol. 38, no. 7, pp. 1505–1511, Jul. 2011.

[36] D. B. Tefelski, T. Piotrowski, V. Blideanu, A. Polański, and J. Skubalski, “Monte-Carlo aided design of neutron shielding concretes,” *Bull. Polish Acad. Sci. Tech. Sci.*, vol. 61, no. 1, pp. 161–171, 2013.

[37] S. J. Stanković, R. D. Ilić, K. Janković, D. Bojović, and B. Lončar, “Gamma Radiation Absorption Characteristics of Concrete with Components of Different Type Materials,” vol. 117, no. 5, pp. 812–816, 2010.

[38] M. E. Medhat, “Comprehensive study of photon attenuation through different construction matters by Monte Carlo simulation,” *Radiat. Phys. Chem.*, vol. 107, pp. 65–74, 2015.

[39] J. Wang, G. Li, and D. Meng, “Evaluation of the performance of peridotite aggregates for radiation shielding concrete,” *Ann. Nucl. Energy*, vol. 71, pp. 436–439, 2014.

[40] S. J. Park, J. G. Jang, and H. K. Lee, “Computational investigation of the neutron shielding and activation characteristics of borated concrete with polyethylene aggregate,” *J. Nucl. Mater.*, vol. 452, no. 1–3, pp. 205–211, 2014.

[41] R. Küçer and N. Küçer, “Neutron Shielding Properties of Concretes Containing Boron Carbide and Ferro – Boron,” vol. 195, pp. 1752–1756, 2015.

[42] T. Piotrowski, M. Mazgaj, A. Żak, and J. Skubalski, “Importance of Atomic Composition and Moisture Content of Cement based Composites in Neutron Radiation Shielding,” *Procedia Engineering*, vol. 108. pp. 616–623, 2015.

[43] S. Agosteo, A. Mereghetti, E. Sagia, and M. Silari, “Shielding data for hadron-therapy ion accelerators: Attenuation of secondary radiation in concrete,” *Nucl. Instruments Methods Phys. Res. Sect. B Beam Interact. with Mater. Atoms*, vol. 319, pp. 154–167, Jan. 2014.

VITA

Raul F. Florez Meza was born in Sincelejo, Colombia in 1989. He studied at the National University of Colombia in Medellin from 2006 until 2011 when he graduated with a B.S in Chemical Engineering. Later in the same year, he was awarded a Youth Research Fellowship Grant by the Colombian research agency COLCIENCIAS. In 2012, Raul joined the Electrochemical Engineering research group "*GRIEQUI"* at the National University of Colombia to conduct research on solid oxide fuel cells. In August 2013, Raul enrolled as a graduate student at Missouri University of Science and Technology at Rolla with the Nuclear Engineering program within the Mining and Nuclear Engineering department. In July 2016, Raul graduated with his Master in Nuclear Engineering.